

# Ultrasonic Velocities, Densities, Viscosities, Electrical Conductivities, Raman Spectra, and Molecular Dynamics Simulations of Aqueous Solutions of $\text{Mg}(\text{OAc})_2$ and $\text{Mg}(\text{NO}_3)_2$ : Hofmeister Effects and Ion Pair Formation

Abdul Wahab,<sup>†</sup> Sekh Mahiuddin,<sup>\*,†</sup> Glenn Hefter,<sup>\*,‡</sup> Werner Kunz,<sup>\*,§</sup> Babak Minofar,<sup>||</sup> and Pavel Jungwirth<sup>\*,||</sup>

Material Science Division, Regional Research Laboratory, Jorhat - 785 006, Assam, India, Department of Chemistry, Murdoch University, Murdoch, WA 6150, Australia, Institut für Physikalische und Theoretische Chemie, Universität Regensburg, D-93040 Regensburg, Germany, and Institute of Organic Chemistry and Biochemistry, Academy of Sciences of the Czech Republic, and Center for Biomolecules and Complex Molecular Systems, Flemingovo nám. 2, 16610 Prague 6, Czech Republic

Received: June 21, 2005; In Final Form: October 18, 2005

The ultrasonic velocities, densities, viscosities, and electrical conductivities of aqueous solutions of magnesium nitrate and magnesium acetate have been measured from dilute to saturation concentrations at  $0 \leq t/^{\circ}\text{C} \leq 50$ . The temperature derivative of the isentropic compressibility,  $\kappa_s$ , became zero at 2.28 and 2.90 mol  $\text{kg}^{-1}$  for  $\text{Mg}(\text{OAc})_2$  and  $\text{Mg}(\text{NO}_3)_2$  solutions, respectively, at 25  $^{\circ}\text{C}$ . The total hydration numbers of the dissolved ions were estimated to be, respectively, 24.3 and 19.2 at these concentrations. Differences in  $\kappa_s$  for various  $\text{M}^{2+}$  salts, using the present and literature data, correlated with reported  $\text{M}^{2+}-\text{OH}_2$  bond lengths and to a lesser extent with cationic charge densities (ionic radii). The influence of anions on  $\kappa_s$  appears to follow the Hofmeister series and also correlates approximately with the anionic charge density. Substantial differences between  $\text{Mg}(\text{OAc})_2(\text{aq})$  and  $\text{Mg}(\text{NO}_3)_2(\text{aq})$  occur with respect to their structural relaxation times (derived from compressibility and viscosity data) and their electrical conductivities. These differences were attributed to a much greater ion association in  $\text{Mg}(\text{OAc})_2$  solutions. Raman spectra recorded at 28  $^{\circ}\text{C}$  confirmed the presence of various types of contact ion pairs including mono- and bidentate complexes in  $\text{Mg}(\text{OAc})_2(\text{aq})$ . In  $\text{Mg}(\text{NO}_3)_2(\text{aq})$ , only noncontact ion pairs appear to be formed even at high concentrations. The experimental results are supported by molecular dynamics simulations, which also reveal the much stronger tendency of  $\text{OAc}^-$  compared to  $\text{NO}_3^-$  to associate with  $\text{Mg}^{2+}$  in aqueous solutions. The simulations also allow an evaluation of the ion–ion and ion–water radial distribution functions and cumulative sums and provide a molecular picture of ion hydration in  $\text{Mg}(\text{OAc})_2(\text{aq})$  and  $\text{Mg}(\text{NO}_3)_2(\text{aq})$  at varying concentrations.

## 1. Introduction

The presence, nature, and concentration of salts can dramatically alter the solubility and behavior of other molecules in solution.<sup>1</sup> Consequently, the solvation of ions in aqueous media is of prime importance in many areas including surface chemistry, environmental chemistry, and geochemistry. In particular, to understand the processes occurring in living cells<sup>2,3</sup> (such as ion transport across cell membranes, the functioning of proteins, and ion channels), the nature of ion hydration is prerequisite information. The hydration of multivalent metal ions is especially interesting because of the presence of well-defined solvation shells and the formation of specific complexes.<sup>4</sup> Magnesium ion is present at moderate concentrations in living cells<sup>5</sup> and seawater<sup>6</sup>, and its salts are important industrially. The acetate ion occurs widely in nature, being produced by microorganisms and by the decomposition of humic acids,<sup>7,8</sup>

while nitrate is of special environmental importance in the atmosphere and in soils.<sup>9</sup>

It is well established<sup>10–16</sup> that six water molecules are strongly bound in the primary hydration shell of  $\text{Mg}^{2+}$  in aqueous solutions. In fact,  $\text{Mg}^{2+}$  retains the hexahydrate structure, with an almost constant  $\text{Mg}^{2+}-\text{(OH}_2)_6$  bond length irrespective of the nature of the counteranion.<sup>12,13</sup> On the basis of X-ray diffraction studies of  $\text{Mg}(\text{NO}_3)_2(\text{aq})$ , Caminiti et al.<sup>12</sup> suggested that nitrate ions do not produce any pronounced structuring effect in their neighborhood. As well as confirming that  $\text{Mg}^{2+}$  has an inner hydration shell of 6, they also proposed a second coordination shell of 12 water molecules, which was also suggested by Bol et al.<sup>10</sup> Conductivity<sup>17</sup> and vapor pressure<sup>18</sup> measurements imply that complex formation between  $\text{Mg}^{2+}$  and  $\text{NO}_3^-$  in aqueous solutions (at concentrations  $m \leq 2.2$  mol  $\text{kg}^{-1}$ ) is unlikely.

Consistent with these measurements, several Raman spectral studies<sup>19–24</sup> have concluded that contact ion pairs do not form in  $\text{Mg}(\text{NO}_3)_2(\text{aq})$  up to saturation (3.85 mol  $\text{dm}^{-3}$ ) at 25  $^{\circ}\text{C}$ . Nevertheless, principal component analysis<sup>25</sup> of Raman spectra has revealed the presence of some associated species at  $M \geq 2.5$  mol  $\text{dm}^{-3}$ , which were earlier assigned to be solvent-shared ion pairs by Chang and Irish.<sup>22</sup> James and Frost<sup>26</sup> reported the

\* To whom correspondence should be addressed. E-mail: mahirrljt@yahoo.com (S.M.); g.hefter@murdoch.edu.au (G.H.); werner.kunz@chemie.uni-regensburg.de (W.K.); pavel.jungwirth@uochb.cas.cz (P.J.).

<sup>†</sup> Regional Research Laboratory.

<sup>‡</sup> Murdoch University.

<sup>§</sup> Universität Regensburg.

<sup>||</sup> Academy of Sciences of the Czech Republic.

existence of solvent-shared ion pairs in this system even at  $\geq 0.5$  mol  $\text{dm}^{-3}$  using a similar approach.

At higher temperatures (up to 120 °C), Peleg<sup>21</sup> showed, again via Raman spectroscopy, that  $\text{Mg}(\text{OH}_2)_6^{2+}$  remained intact, as suggested by Angell,<sup>27</sup> at concentrations  $\leq 9.25$  mol  $\text{kg}^{-1}$  but, beyond that,  $\text{NO}_3^-$  entered the primary hydration shell of  $\text{Mg}^{2+}$ . Peleg also reported the existence of a perturbed quasi-lattice structure for  $\text{Mg}^{2+}-\text{NO}_3^-$  contact ion pairs in  $\text{Mg}(\text{NO}_3)_2 \cdot 2.4\text{H}_2\text{O}$  and  $\text{Mg}(\text{NO}_3)_2 \cdot 2\text{H}_2\text{O}$  melts. Irish et al.<sup>28</sup> proposed the presence of two bidentate contact ion pairs:  $[\text{Mg}^{2+}(\text{H}_2\text{O})_4(\text{NO}_3^-)]$  and  $[\text{Mg}^{2+}(\text{H}_2\text{O})_2(\text{NO}_3^-)_2]$  in  $\text{Mg}(\text{NO}_3)_2 \cdot 2.2\text{H}_2\text{O}$  melts. Chang and Irish<sup>22</sup> later identified contact ion pairs in 9.25 mol  $\text{kg}^{-1}$   $\text{Mg}(\text{NO}_3)_2 \cdot 6\text{H}_2\text{O}$  and inferred that a monodentate to bidentate conversion occurs as water is further removed. Very recently, Zhang et al.<sup>23</sup> studied aqueous  $\text{Mg}(\text{NO}_3)_2$  droplets using an electrodynamic balance in conjunction with Raman spectroscopy and observed a large variety of contact ion pairs including monodentate and bidentate species.

Aqueous solutions of  $\text{Mg}(\text{OAc})_2$  appear particularly interesting with respect to the formation of different types of species at different concentrations. Caminiti et al.<sup>29</sup> reported the presence of a monoacetato complex in 0.25–1.5 mol  $\text{dm}^{-3}$  aqueous  $\text{Mg}(\text{OAc})_2$  solutions, employing X-ray scattering and  $^{13}\text{C}$  NMR spectroscopy. Conductivity studies in very dilute solutions ( $\leq 0.002$  mol  $\text{dm}^{-3}$ ) indicate ion association in  $\text{Mg}(\text{OAc})_2(\text{aq})$  with a modest association constant,  $K_A^\circ$ , for 1:1 stoichiometry, of  $\approx 50$   $\text{dm}^3 \text{mol}^{-1}$ .<sup>30</sup> An ultrasonic absorption study<sup>31</sup> suggested that  $\text{OAc}^-$  did not penetrate into the primary hydration shell of  $\text{Mg}^{2+}$ .

Investigating the symmetric and antisymmetric stretching modes of the carboxylate group by attenuated total reflection (ATR)-IR spectroscopy, Tackett<sup>32</sup> observed only free ions in dilute (0.6 mol  $\text{dm}^{-3}$ )  $\text{Mg}(\text{OAc})_2(\text{aq})$ . Semmler et al.<sup>8</sup> studied the C–C stretching modes in the Raman spectra of  $\text{OAc}^-$  at a pressure of 9 MPa and temperatures up to 150 °C in solutions containing  $\text{MgCl}_2$ ,  $\text{Mg}(\text{OAc})_2$ ,  $\text{NaOAc}$ , and  $\text{NaNO}_3$  having total mole ratios of  $\text{OAc}^-$  to  $\text{Mg}^{2+}$  of 0.5 to 6 and suggested the existence of two monodentate complexes. Nickolov et al.<sup>33</sup> reported the existence of mono- and bisacetato complexes in 0.65–3.24 mol  $\text{dm}^{-3}$   $\text{Mg}(\text{OAc})_2$  solutions from Raman measurements. Using ATR-IR and Raman spectra of dilute (0.05–0.6 mol  $\text{dm}^{-3}$ )  $\text{Mg}(\text{OAc})_2$ , Quilès and Burneau<sup>34</sup> found no contact ion pairs, consistent with Tackett.<sup>32</sup> Very recently, Wang et al.<sup>35</sup> studied supersaturated  $\text{Mg}(\text{OAc})_2(\text{aq})$  droplets ( $m \geq 3.58$  mol  $\text{kg}^{-1}$ ) using a droplet levitation technique with in-situ Raman spectroscopy. They detected bidentate complexes and also proposed the formation of bridged bidentate complexes. For a better overview, the various species reported in aqueous solutions of  $\text{Mg}(\text{NO}_3)_2$  and  $\text{Mg}(\text{OAc})_2$  are summarized in Table 1.

Solutions of acetate and nitrate salts at moderate concentrations are also of interest in connection with the ubiquitous, but largely unexplained, Hofmeister series. This series of ions, established originally on the basis of their effects on protein solubilities,<sup>36</sup> has been observed in an impressive range of biological and biochemical phenomena.<sup>37</sup> However, despite some recent progress,<sup>38</sup> understanding of this series remains obscure and few papers deal with other than monovalent ions. Since  $\text{OAc}^-$  and  $\text{NO}_3^-$  lie toward the two extremes of the Hofmeister series (salting-out and salting-in, respectively), it is of interest to compare their physicochemical properties, which may shed light on this important topic.

It has long been postulated that, when an electrolyte is added in water, the constituent ions markedly modify the water

**TABLE 1: Different Ionic Species Present in Salt Solutions Obtained from Raman Spectra (R), IR Spectra (IR), NMR Spectra (NMR), X-ray Diffraction (X), Conductivity (C), Vapor Pressure (V), Hygroscopicity (H), and Ultrasonic Absorption (UA) Methods at Ambient Temperatures**

solute	concentration	ionic species	method	ref
$\text{Mg}(\text{NO}_3)_2$	1.0, 2.0, 4.0 M, <sup>a</sup>	no complexes detected	X	10,12
	very dilute	little association	C	17
	$\leq 2.197 \text{ m}^a$	little association	V	18
	2.77–9.25 m	solvent-shared ion pairs	R	21
	$\geq 9.25 \text{ m}$	contact ion pairs <sup>b</sup>	R	21
	2.8–4.9 m	solvent-shared ion pairs	R	22
	$\geq 9.25 \text{ m}$	mono- and bidentate complexes <sup>c</sup>	R	22
	6–2.0 WSR <sup>a</sup>	mono- and bidentate complexes	R and H	23
	2.2 WSR	bidentate complexes <sup>d</sup>	R	28
	$\geq 2.5 \text{ M}$	associated species	R	25
	0.5–3.0 M	solvent-shared ion pairs	R	26
	0.05–0.6 M	no complexes detected	IR and R	34
	0.6 M	no complexes detected	IR	32
	$\leq 0.002 \text{ M}$	1:1 complex	C	30
$\text{Mg}(\text{OAc})_2$	0.65–3.24 M	mono- and bisacetato complexes	R	33
	0.501–5.98 MR <sup>a</sup>	monodentate complexes	R	8
	0.25–1.5 M	monodentate complex	X and NMR	29
	$\leq 0.4 \text{ M}$	no contact ion pairs	UA	31
	15.5–2.58 WSR	mono- and bidentate complexes	R and H	35

<sup>a</sup>  $m$  = mol  $\text{kg}^{-1}$ ,  $M$  = mol  $\text{dm}^{-3}$ , WSR = water-to-solute ratio, MR =  $\text{OAc}^-$  to  $\text{Mg}^{2+}$  molar ratio. <sup>b</sup>  $\leq 120$  °C. <sup>c</sup> 150–200 °C. <sup>d</sup>  $> 100$  °C.

structure (hydrogen bonding), which affects the physicochemical properties of the solution.<sup>39</sup> Recent studies<sup>40</sup> contradict this century old understanding and showed that ions do not influence the water structure of the bulk water (second hydration sphere onward) but only the hydrogen bonding of the water in the immediate vicinity of ions, that is, water in the first hydration sphere, is broken or formed.

This paper presents a detailed study of the ultrasonic velocities, densities, viscosities, and electrical conductivities of aqueous solutions of  $\text{Mg}(\text{NO}_3)_2$  and  $\text{Mg}(\text{OAc})_2$  from dilute to saturation concentrations and as a function of temperature. Fourier transform (FT)-Raman spectra of these solutions have also been recorded to clarify the role of ion association. The experimental data are complemented by molecular dynamics simulations of aqueous solutions of  $\text{Mg}(\text{NO}_3)_2$  and  $\text{Mg}(\text{OAc})_2$  at 0.25 and 1 M concentrations. These calculations, which employ periodic boundary conditions to simulate the aqueous bulk, provide a picture with atomic resolution of solvation of individual ions and allow quantification of the degree of ion pairing in the magnesium nitrate vs acetate solutions in terms of ion–ion pair distribution functions.

## 2. Experimental Section

$\text{Mg}(\text{OAc})_2 \cdot 4\text{H}_2\text{O}$  ( $> 99\%$ , SRL, India) and  $\text{Mg}(\text{NO}_3)_2 \cdot 6\text{H}_2\text{O}$  ( $> 99\%$ , SD Fine Chemicals, India) were recrystallized twice from double-distilled water and then kept in a vacuum desiccator over  $\text{P}_2\text{O}_5$ . All solutions were prepared using double-distilled water and by the successive dilution of a stock solution. The concentrations were finally checked by complexometric titration against EDTA.<sup>41</sup> The overall accuracy in the solution preparation was within  $\pm 0.3\%$ .

The detailed measurement procedures for ultrasonic velocities at 3 MHz, densities, and viscosities are described elsewhere.<sup>42–44</sup> The uncertainties in the measurements of ultrasonic velocity, density, and viscosity were within  $\pm 0.01\%$ ,  $\pm 0.01\%$ , and  $\pm 0.5\%$ , respectively. Electrical conductivities were measured using platinized platinum electrodes and a Precision Component

Analyzer 6440A (Wayne Kerr, U.K.) at a field frequency of 1 kHz. The cell constant of  $1.237 \text{ cm}^{-1}$  was determined by using a  $0.1 \text{ mol kg}^{-1}$  aqueous KCl solution at different temperatures. The experimental uncertainty in the conductivity values was less than  $\pm 0.4\%$ .

Electrical conductivities, ultrasonic velocities, and viscosities of both systems were measured from 0 to  $50^\circ\text{C}$  at  $5^\circ\text{C}$  intervals as functions of salt concentration ( $0.0145 \leq m/\text{mol kg}^{-1} \leq 6.545$ ). Schott-Geräte CT 1450 or Julabo F32 HP thermostats were used to control solution temperatures to within  $\pm 0.02^\circ\text{C}$ .

FT-Raman spectra of aqueous solutions of  $\text{Mg}(\text{NO}_3)_2$  and  $\text{Mg}(\text{OAc})_2$  were recorded at room temperature ( $28^\circ\text{C}$ ) using a Bruker IFS 66 V optical bench with a FRA 106 Raman module attachment and a Nd:YAG laser operating at  $1064 \text{ nm}$ . The laser power was set at  $200 \text{ mW}$ , and 250 scans were accumulated and averaged with a resolution of  $2 \text{ cm}^{-1}$ . The spectra were recorded at the Sophisticated Analytical Instrumentation Facility, Indian Institute of Technology, Madras, India.

### 3. Computational Details

Classical molecular dynamics simulations of concentrated solutions of magnesium nitrate and magnesium acetate were performed. The unit cell contained 863 water molecules, 4 or 16 magnesium cations, and 8 or 32 nitrate or acetate anions, which corresponds to a  $0.25$  or  $1 \text{ M}$  salt concentration. The size of the cubic unit cell was approximately  $30 \times 30 \times 30 \text{ \AA}$ , and standard periodic boundary conditions were applied.<sup>45</sup> A  $12 \text{ \AA}$  cutoff was used for intermolecular interactions. Long-range Coulombic interactions were accounted for using the particle mesh Ewald procedure.<sup>46</sup> Simulations were run in the NPT canonical ensemble at  $300 \text{ K}$  and  $1 \text{ atm}$ . A time step of  $1 \text{ fs}$  was employed, and all bonds involving hydrogen atoms were constrained using the SHAKE algorithm.<sup>47</sup> All systems were first equilibrated for  $500 \text{ ps}$ , after which a  $1 \text{ ns}$  production run followed.

A nonpolarizable force field was employed in all simulations. Technically, this is the simplest way to avoid the problem of a "polarization catastrophe",<sup>48</sup> which is particularly severe in the presence of multiply charged ions. Physically, this choice can be at least partially justified by the fact that in this study the interest is in the bulk properties of aqueous ions, which are less influenced by specific polarization effects than the interfacial ionic behavior.<sup>49</sup> For water, the SPCE model, which accounts for mean polarization effects by increasing the partial charges on oxygen and hydrogens,<sup>50</sup> was employed. For ions, the general amber force field parameter set was used.<sup>51</sup> For  $\text{Mg}^{2+}$ , which is missing from this set, OPLS parameters were employed.<sup>52</sup> Partial charges for acetate and nitrate were evaluated using the standard RESP procedure employing the Gaussian 03 program,<sup>53</sup> and all molecular dynamics (MD) simulations were performed using the Amber 8 program.<sup>54</sup> To directly check the effect of polarization interaction, several test calculations using a polarizable force field<sup>55,56</sup> were also performed, with an imposed cutoff on induced dipoles in order to avoid the polarization catastrophe,<sup>57</sup> and compared with nonpolarizable simulations. The use of an empirical force field excludes studying the acid/base properties of the acetate ion, since this involves the breaking/making of a chemical bond and, consequently, this is not considered in our simulations.

### 4. Results and Discussion

**4.1. Densities and Isentropic Compressibilities.** Within the limited temperature range investigated, the measured densities,  $\rho$ , of aqueous solutions of  $\text{Mg}(\text{NO}_3)_2$  and  $\text{Mg}(\text{OAc})_2$  were found

**TABLE 2: Least-Squares Fitted Values of the Density Equation,  $\rho = a - bt$ , for Aqueous Solutions of  $\text{Mg}(\text{OAc})_2$  and  $\text{Mg}(\text{NO}_3)_2$  up to Near-Saturation Concentrations**

$m/(\text{mol kg}^{-1})$	$a/(\text{kg m}^{-3})$	$b/(\text{kg m}^{-3} ^\circ\text{C}^{-1})$	std dev in $\rho/(\text{kg m}^{-3})$
Magnesium Acetate			
0.0414	$1010.1 \pm 0.4$	$0.3772 \pm 0.0107$	0.2
0.0831	$1012.9 \pm 0.5$	$0.3686 \pm 0.0120$	0.2
0.1671	$1018.6 \pm 0.5$	$0.3541 \pm 0.0132$	0.3
0.4247	$1038.0 \pm 0.4$	$0.3667 \pm 0.0115$	0.3
0.6460	$1054.4 \pm 0.4$	$0.3898 \pm 0.0093$	0.2
0.8751	$1068.4 \pm 0.4$	$0.3800 \pm 0.0113$	0.3
1.106	$1085.3 \pm 0.4$	$0.4046 \pm 0.0102$	0.2
1.354	$1099.3 \pm 0.4$	$0.4075 \pm 0.0101$	0.2
1.608	$1116.0 \pm 0.3$	$0.4408 \pm 0.0086$	0.2
1.866	$1128.9 \pm 0.3$	$0.4331 \pm 0.0085$	0.2
2.134	$1144.2 \pm 0.3$	$0.4603 \pm 0.0078$	0.2
2.411	$1159.4 \pm 0.4$	$0.4647 \pm 0.0100$	0.2
2.622	$1168.9 \pm 0.3$	$0.4932 \pm 0.0083$	0.2
3.043	$1188.1 \pm 0.3$	$0.5109 \pm 0.0068$	0.1
3.437	$1209.8 \pm 0.2$	$0.5456 \pm 0.0066$	0.1
3.819	$1222.8 \pm 0.3$	$0.5775 \pm 0.0078$	0.2
4.547	$1248.5 \pm 0.2$	$0.6190 \pm 0.0056$	0.1
5.165	$1269.1 \pm 0.3$	$0.6599 \pm 0.0066$	0.1
5.732	$1285.6 \pm 0.2$	$0.6810 \pm 0.0064$	0.1
6.187	$1300.4 \pm 0.2$	$0.7305 \pm 0.0034$	0.1
6.545	$1309.1 \pm 0.2$	$0.7519 \pm 0.0048$	0.1
Magnesium Nitrate			
0.0145	$1008.0 \pm 0.5$	$0.3686 \pm 0.0130$	0.2
0.0528	$1012.2 \pm 0.4$	$0.3682 \pm 0.0109$	0.2
0.2491	$1034.3 \pm 0.4$	$0.4106 \pm 0.0114$	0.2
0.3405	$1042.0 \pm 0.4$	$0.3869 \pm 0.0101$	0.2
0.5931	$1068.2 \pm 0.3$	$0.4287 \pm 0.0087$	0.2
0.6173	$1072.0 \pm 0.3$	$0.4542 \pm 0.0062$	0.1
0.8960	$1099.2 \pm 0.3$	$0.4696 \pm 0.0074$	0.1
0.9898	$1109.0 \pm 0.3$	$0.4884 \pm 0.0067$	0.1
1.262	$1133.7 \pm 0.3$	$0.5079 \pm 0.0077$	0.1
1.525	$1157.2 \pm 0.1$	$0.5270 \pm 0.0031$	0.1
1.694	$1172.8 \pm 0.2$	$0.5444 \pm 0.0045$	0.1
1.827	$1186.2 \pm 0.2$	$0.5611 \pm 0.0052$	0.1
2.131	$1211.3 \pm 0.2$	$0.5659 \pm 0.0047$	0.1
2.493	$1240.1 \pm 0.2$	$0.5918 \pm 0.0060$	0.1
2.584	$1248.5 \pm 0.1$	$0.5943 \pm 0.0040$	0.1
2.793	$1264.2 \pm 0.1$	$0.6039 \pm 0.0034$	0.1
3.096	$1287.0 \pm 0.1$	$0.6177 \pm 0.0040$	0.1
3.118	$1288.1 \pm 0.2$	$0.6219 \pm 0.0048$	0.1
3.170	$1296.7 \pm 0.2$	$0.6169 \pm 0.0043$	0.1
3.501	$1315.2 \pm 0.1$	$0.6242 \pm 0.0043$	0.1
3.704	$1329.0 \pm 0.1$	$0.6338 \pm 0.0032$	0.1
3.757	$1332.3 \pm 0.1$	$0.6388 \pm 0.0028$	0.1
4.039	$1350.0 \pm 0.1$	$0.6441 \pm 0.0032$	0.1
4.051	$1349.5 \pm 0.1$	$0.6269 \pm 0.0033$	0.1
4.285	$1366.4 \pm 0.1$	$0.6422 \pm 0.0029$	0.1
4.403	$1373.6 \pm 0.1$	$0.6475 \pm 0.0020$	0.1
4.728	$1395.4 \pm 0.1$	$0.6532 \pm 0.0027$	0.1
4.883	$1402.2 \pm 0.1$	$0.6569 \pm 0.0025$	0.1
4.970	$1408.4 \pm 0.1$	$0.6579 \pm 0.0027$	0.1
5.134	$1419.6 \pm 0.2$	$0.6668 \pm 0.0049$	0.1
5.282	$1427.2 \pm 0.5$	$0.6401 \pm 0.0127$	0.2

to vary linearly with temperature at a fixed concentration. The least-squares fitted values of the parameters of the density equation ( $\rho = a - bt$ ) are listed in Table 2. The present densities at  $25^\circ\text{C}$  agree within  $\pm 0.2\%$  with literature<sup>58–60</sup> data for both  $\text{Mg}(\text{OAc})_2$  and  $\text{Mg}(\text{NO}_3)_2$  solutions. The corresponding ultrasonic velocities,  $u$ , were comparable within  $\pm 0.2\%$  for  $\text{Mg}(\text{OAc})_2(\text{aq})$  and  $\pm 0.4\%$  for  $\text{Mg}(\text{NO}_3)_2(\text{aq})$  with literature<sup>58,61</sup> data at  $25^\circ\text{C}$ .

Isentropic compressibilities,  $\kappa_s$ , of  $\text{Mg}(\text{OAc})_2(\text{aq})$  and  $\text{Mg}(\text{NO}_3)_2(\text{aq})$  were calculated using

$$\kappa_s = (u^2 \rho)^{-1} \quad (1)$$

and are plotted against concentration for the three temperatures in Figure 1. Because of the wide concentration range of interest here, an empirical equation<sup>42,43</sup> was used to describe the  $\kappa_s$  values. The parameters so obtained are summarized in Table 3.



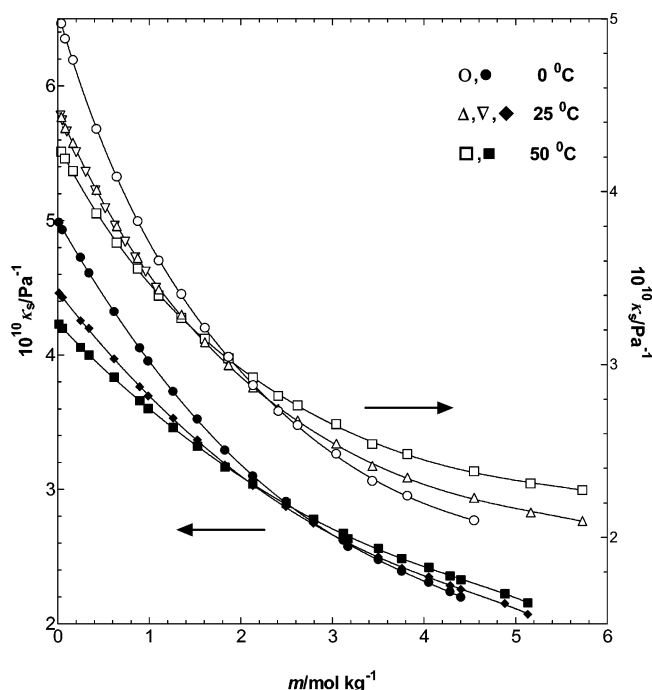


**Figure 1.** Isentropic compressibilities of aqueous solutions of Mg(OAc)<sub>2</sub> (open symbols) and Mg(NO<sub>3</sub>)<sub>2</sub> (solid symbols) as a function of concentration and temperature. Solid curves are calculated from the isentropic compressibility equation,  $\kappa_s = a_1 + b_1m + c_1m^{1.5} + d_1m^2 + e_1m^{2.5} + f_1m^3$  (see ref 43),  $\nabla$  ref 58.

Figure 1 and Table 3 show that the equation can reproduce the data within the 95% confidence level.

It is apparent from Figure 1 that the  $\kappa_s$  isotherms for each electrolyte within the studied temperature range (0–50 °C) exhibit a crossover at an approximately constant concentration that appears to be characteristic. As the electrolyte concentration increases,  $\kappa_s$  decreases due to the simultaneous effects of ion hydration and the modification of water molecules located in the direct vicinity of the ions. The main contributor to these effects would be expected to be Mg<sup>2+</sup> because of its higher charge density and hydration energy.<sup>62</sup>

A long-standing assumption of solution chemistry is that the addition of electrolytes (ions) to water significantly alters the water structure, which is reflected in the changes in the physicochemical properties (viscosity, surface tension, etc.) of the solutions so formed. But recent reports suggest that ions only influence the hydrogen bonding of water molecules in their immediate vicinity, that is, the water molecules in the primary hydration shell.<sup>40</sup>

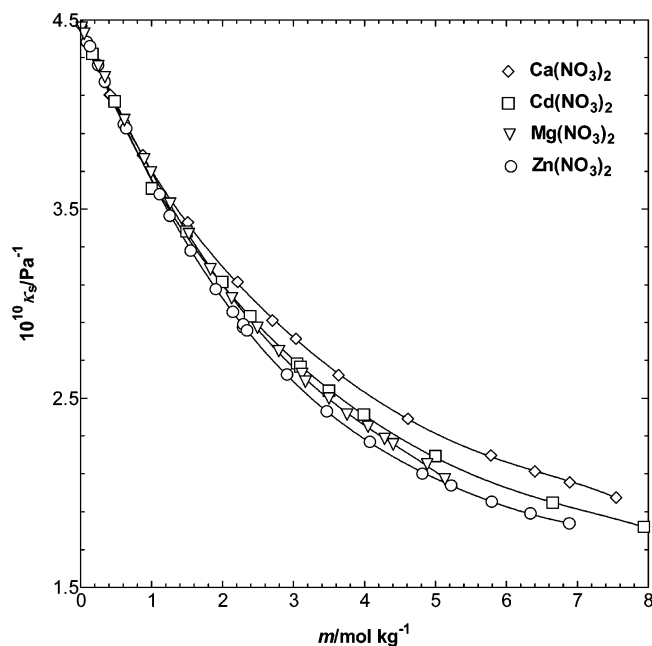


**Figure 2.** Isentropic compressibilities of various aqueous solutions of NO<sub>3</sub><sup>−</sup> salts as a function of concentration at 25 °C:  $\circ$  ref 42,  $\square$  and  $\diamond$  ref 43.

The influence of cations on  $\kappa_s$  is illustrated in Figure 2, which plots  $\kappa_s$  for aqueous solutions of various metal nitrate salts at 25 °C. As would be expected from the greater electrostriction<sup>63</sup> associated with decreasing cationic radii ( $r$ ),<sup>39</sup> the  $\kappa_s$  values at higher solute concentrations increase in the order of their M<sup>2+</sup>–OH<sub>2</sub> distances ( $d$ ) ( $d = 2.04, 2.12, 2.31$ , and  $2.44$  Å for M = Mg, Zn, Cd, and Ca, respectively)<sup>64</sup> with Mg<sup>2+</sup> as a partial exception.

On the other hand, comparison of the effects of anions on  $\kappa_s$  values is less straightforward. Figure 3 shows that Mg(OAc)<sub>2</sub> solutions are less compressible than Mg(NO<sub>3</sub>)<sub>2</sub> solutions up to  $\approx 4.6$  mol kg<sup>−1</sup> at 25 °C but this is reversed at higher concentrations. For comparison,  $\kappa_s$  data for MgCl<sub>2</sub> and MgSO<sub>4</sub> solutions<sup>65</sup> are also included in Figure 3. In contrast with the cations, the  $\kappa_s$  values do not correlate with the anion–water distances ( $d(\text{SO}_4^{2-}-(\text{H}_2\text{O})) = 3.70$  Å,  $d(\text{OAc}^{−}-(\text{H}_2\text{O})) = 3.70$  Å,  $d(\text{Cl}^{−}-(\text{H}_2\text{O})) = 3.15$  Å,  $d(\text{NO}_3^{−}-(\text{H}_2\text{O})) = 3.40$  Å) obtained from diffraction studies.<sup>12,13</sup>

It is noteworthy that the  $\kappa_s$  data as presented appear to conform to the Hofmeister series.<sup>36</sup> OAc<sup>−</sup> and SO<sub>4</sub><sup>2−</sup> belong to the salting-out side, Cl<sup>−</sup> is in the middle, and NO<sub>3</sub><sup>−</sup> belongs to the salting-in side of the series. On this basis, Mg(OAc)<sub>2</sub> and Mg(NO<sub>3</sub>)<sub>2</sub> would be expected to have qualitatively different

**TABLE 3: Values of the Parameters of the Isentropic Compressibility Equation,  $\kappa_s = a_1 + b_1m + c_1m^{1.5} + d_1m^2 + e_1m^{2.5} + f_1m^3$  (see ref 43), for Aqueous Solutions of Mg(OAc)<sub>2</sub> and Mg(NO<sub>3</sub>)<sub>2</sub>**

parameters	0 °C	25 °C	50 °C
Magnesium Acetate			
$10^{10}a_1/\text{Pa}^{-1}$	$5.0403 \pm 0.0076$	$4.4759 \pm 0.0059$	$4.2758 \pm 0.0057$
$10^{10}b_1/\text{Pa}^{-1} \text{ kg mol}^{-1}$	$-1.8405 \pm 0.0459$	$-1.2317 \pm 0.0268$	$-1.0471 \pm 0.0259$
$10^{10}c_1/\text{Pa}^{-1} \text{ kg}^{1.5} \text{ mol}^{-1.5}$	$0.6508 \pm 0.0713$	$0.3344 \pm 0.0326$	$0.2954 \pm 0.0314$
$10^{10}d_1/\text{Pa}^{-1} \text{ kg}^2 \text{ mol}^{-2}$	$-0.1728 \pm 0.0424$	$-0.0690 \pm 0.0153$	$-0.0636 \pm 0.0147$
$10^{10}e_1/\text{Pa}^{-1} \text{ kg}^{2.5} \text{ mol}^{-2.5}$	$0.0271 \pm 0.0106$	$0.0093 \pm 0.0030$	$0.0086 \pm 0.0029$
$10^{12}f_1/\text{Pa}^{-1} \text{ kg}^3 \text{ mol}^{-3}$	$-0.0017 \pm 0.0009$	$-0.0005 \pm 0.0002$	$-0.0005 \pm 0.0002$
$10^{10}\sigma/\text{std. dev.}$	0.0075	0.0066	0.0064
Magnesium Nitrate			
$10^{10}a_1/\text{Pa}^{-1}$	$5.0008 \pm 0.0067$	$4.4750 \pm 0.0611$	$4.2374 \pm 0.0050$
$10^{10}b_1/\text{Pa}^{-1} \text{ kg mol}^{-1}$	$-1.1907 \pm 0.0391$	$-0.8908 \pm 0.0302$	$-0.7278 \pm 0.0248$
$10^{10}c_1/\text{Pa}^{-1} \text{ kg}^{1.5} \text{ mol}^{-1.5}$	$0.1115 \pm 0.0011$	$0.1273 \pm 0.0407$	$0.1106 \pm 0.0334$
$10^{10}d_1/\text{Pa}^{-1} \text{ kg}^2 \text{ mol}^{-2}$	$-0.0011 \pm 0.0367$	$-0.0199 \pm 0.0210$	$-0.0262 \pm 0.0173$
$10^{10}e_1/\text{Pa}^{-1} \text{ kg}^{2.5} \text{ mol}^{-2.5}$	$0.0009 \pm 0.0094$	$0.0044 \pm 0.0046$	$0.0062 \pm 0.0038$
$10^{12}f_1/\text{Pa}^{-1} \text{ kg}^3 \text{ mol}^{-3}$	$-0.0002 \pm 0.0008$	$-0.0004 \pm 0.0004$	$-0.0006 \pm 0.0006$
$10^{10}\sigma/\text{std. dev.}$	0.0075	0.0071	0.0058

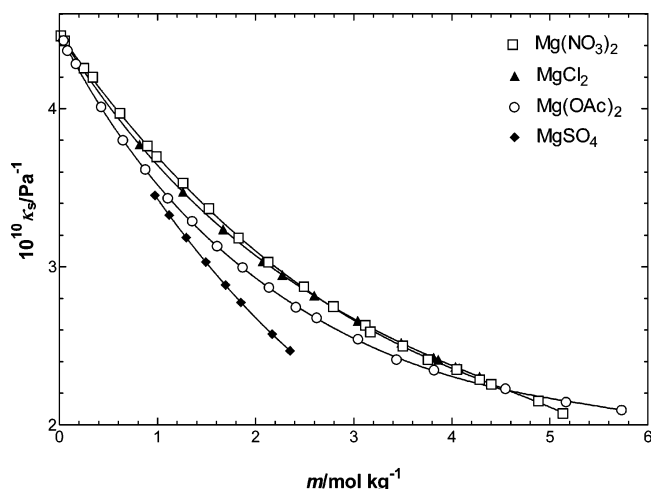


**Figure 3.** Isentropic compressibilities of aqueous solutions of various  $\text{Mg}^{2+}$  salts as a function of concentration at 25 °C:  $\blacktriangle$  and  $\blacklozenge$  ref 65.

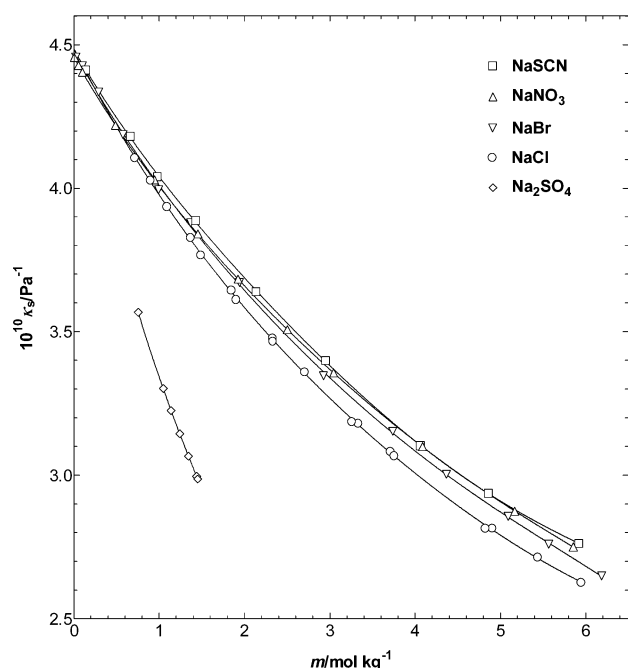


**Figure 4.** Isentropic compressibilities of aqueous solutions of various  $\text{Na}^+$  salts as a function of concentration at 25 °C:  $\square$  ref 44,  $\circ$ ,  $\diamond$  ref 65,  $\triangle$  ref 68, and  $\nabla$  ref 69.

effects on the water molecules located in the first hydration shell in the immediate vicinity of ions. As discussed above (Figure 1), the crossover concentration for  $\text{Mg}(\text{OAc})_2(\text{aq})$  is lower than that for  $\text{Mg}(\text{NO}_3)_2(\text{aq})$ , which implies that  $\text{OAc}^-$  is more efficient in influencing the water molecules in its first hydration sphere than  $\text{NO}_3^-$ . Further, the values of the estimated viscosity A- and B-coefficients, using the extended Jones–Dole equation<sup>66,67</sup> for  $\text{Mg}(\text{NO}_3)_2(\text{aq})$  and  $\text{Mg}(\text{OAc})_2(\text{aq})$ , were estimated to be 0.0017 and 0.0074  $\text{dm}^{3/2} \text{mol}^{-1/2}$  and 0.0022 and 0.217  $\text{dm}^3 \text{mol}^{-1}$ , respectively. The higher values of the viscosity A- and B-coefficients of  $\text{Mg}(\text{OAc})_2(\text{aq})$  suggest that  $\text{OAc}^-$  forms a more rigid structure with water molecules in the first hydration shell due to strong solvation of ions,<sup>67</sup> which is reflected in Figure 1.

To further investigate possible Hofmeister effects, Figure 4 plots  $\kappa_s$  values at 25 °C for various Na salts.<sup>44,65,68,69</sup> The trend is again consistent with the Hofmeister series, taking the data at face value.<sup>36</sup>

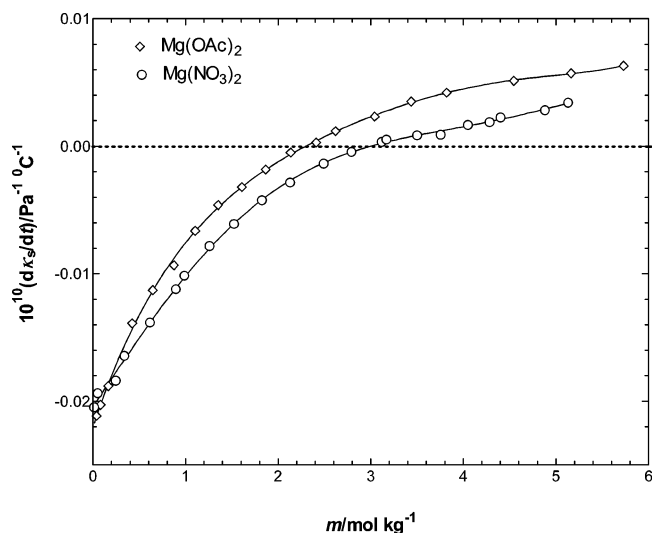


**Figure 5.** Temperature derivative of isentropic compressibility as a function of concentration for aqueous solutions of  $\text{Mg}(\text{OAc})_2$  and  $\text{Mg}(\text{NO}_3)_2$  at 25 °C.

The crossover concentration for  $\kappa_s$  isotherms (Figure 1) can be considered<sup>42,43</sup> as coinciding with the disappearance of the bulk water structure, with all the water molecules being incorporated into the first hydration shells of the ions, resulting in a more rigid structure for the solution. Beyond this concentration, the co-spheres of the cations and anions overlap leading to the formation of ion pairs.<sup>70</sup> Figure 1 shows that the  $\kappa_s$  isotherms for  $\text{Mg}(\text{OAc})_2$  and  $\text{Mg}(\text{NO}_3)_2$  solutions do not cross at a fixed concentration but rather over narrow concentration ranges (1.50–2.30  $\text{mol kg}^{-1}$  and 2.00–3.00  $\text{mol kg}^{-1}$ , respectively) within the temperature range of study. To estimate the total hydration number of the ions at 25 °C, a plot of the temperature derivative of  $\kappa_s$  for both systems was made; see Figure 5. A two-degree polynomial equation was used to fit the data. Evidently, the  $d\kappa_s/dt$  plots become zero at 2.28  $\text{mol kg}^{-1}$  and 2.90  $\text{mol kg}^{-1}$ , respectively, for  $\text{Mg}(\text{OAc})_2$  and  $\text{Mg}(\text{NO}_3)_2$  solutions.

The total hydration numbers,  $n_h$ , of  $\text{Mg}(\text{OAc})_2(\text{aq})$  and  $\text{Mg}(\text{NO}_3)_2(\text{aq})$  can be calculated using the empirical equation<sup>42–44</sup>

$$n_h = (\kappa_{s,\phi} - \kappa_{s,h}V_\phi) / [V_0(\kappa_{s,h} - \kappa_{s,0})] \quad (2)$$

where  $\kappa_{s,\phi} (= (1/m\rho_0)(\kappa_s - \kappa_{s,0}) + \kappa_s V_\phi$ , where  $m$  is the concentration in  $\text{mol kg}^{-1}$  and  $\rho_0$  and  $\kappa_{s,0}$  are the density and the isentropic compressibility of the solvent, respectively) is the apparent molal isentropic compressibility of the solute,  $\kappa_{s,h}$  is the isentropic compressibility of the hydration shell of the solute,  $V_\phi (= M/\rho - (\rho - \rho_0)/\rho\rho_0m$ , where  $M$  is the molar mass of the solute) is the apparent molal volume of the solute, and  $V_0 (= M_0/\rho_0$ , where  $M_0$  is the molar mass of the solvent) is the molar volume of the solvent. Through the use of this expression, the total hydration numbers for  $\text{Mg}(\text{OAc})_2$  and  $\text{Mg}(\text{NO}_3)_2$  solutions were estimated to be 24.3 and 19.2 at 2.28 and 2.90  $\text{mol kg}^{-1}$ , respectively.

**4.2. Structural Relaxation Times.** The measured viscosities for  $\text{Mg}(\text{NO}_3)_2(\text{aq})$  are within  $\pm 5\%$  of the literature values.<sup>59,60</sup> No previous viscosity data appear to have been published for  $\text{Mg}(\text{OAc})_2(\text{aq})$ .

To help understand the nature of ionic interactions at different concentrations, the structural relaxation time,  $\tau$ , was calculated using

$$\tau = 4\kappa_s\eta/3 \quad (3)$$

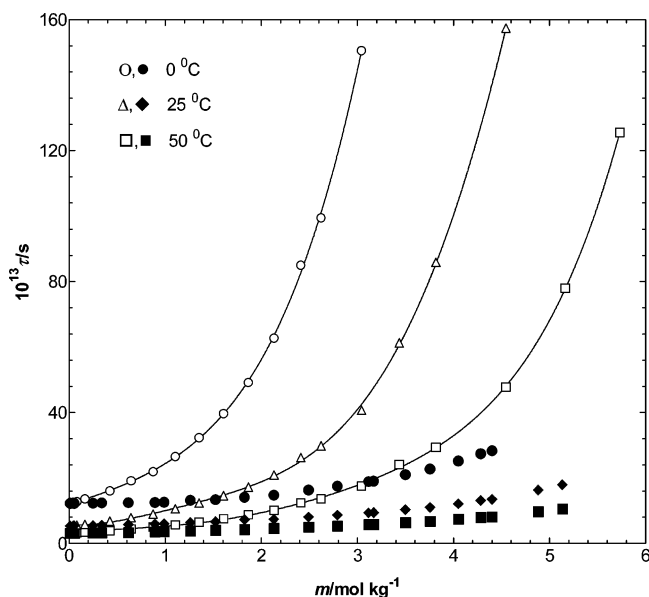


**Figure 6.** Variation of the structural relaxation time,  $\tau$ , with concentration for aqueous solutions of  $\text{Mg}(\text{OAc})_2$  (open symbols) and  $\text{Mg}(\text{NO}_3)_2$  (solid symbols).

The quantity  $\tau$  can be considered as the time required to relieve the shear stress at constant strain through viscous flow. It is particularly sensitive to the formation of ion pairs because of coupling between ion–solvent and ion–ion interactions. Figure 6 shows the variation of  $\tau$  with concentration at three temperatures for aqueous solutions of  $\text{Mg}(\text{NO}_3)_2$  and  $\text{Mg}(\text{OAc})_2$ .

The dramatic differences between the solutions of the two salts almost certainly reflect the differences in the extent and nature of their ion association. Although the existing information (Table 1) is somewhat contradictory, there is little doubt that  $\text{Mg}(\text{OAc})_2(\text{aq})$  not only is more strongly associated than  $\text{Mg}(\text{NO}_3)_2(\text{aq})$  but also forms more contact (inner sphere) species. These issues will be discussed further below when considering the Raman spectra.

**4.3. Electrical Conductivities.** If ion pair formation in  $\text{Mg}(\text{OAc})_2(\text{aq})$  is significantly greater than in  $\text{Mg}(\text{NO}_3)_2(\text{aq})$ , then measurable effects on ionic mobilities, that is, on their electrical conductivities,  $\kappa$ , for aqueous solutions of  $\text{Mg}(\text{OAc})_2$  and  $\text{Mg}(\text{NO}_3)_2$  are around 3–6%<sup>71a</sup> and 1–10%,<sup>71b</sup> respectively, lower than the literature values at 25 °C.

Figure 7 plots  $\kappa$  vs  $m$  for solutions of the two salts at three temperatures. All the  $\kappa$  isotherms pass through a maximum ( $\kappa_{\text{max}}$ ), which is located at  $1.07 \pm 0.13$  and  $2.45 \pm 0.09$  mol  $\text{kg}^{-1}$  for the acetate and nitrate salts, respectively. At higher concentrations ( $> 1$  mol  $\text{kg}^{-1}$ ),  $\kappa(\text{Mg}(\text{OAc})_2(\text{aq}))$  is substantially smaller than  $\kappa(\text{Mg}(\text{NO}_3)_2(\text{aq}))$ . Although a small part of these differences can be attributed to the greater mobility of  $\text{NO}_3^-$ ,  $\lambda^\circ(\text{NO}_3^-) = 71.5$   $\text{cm}^2$   $\text{S mol}^{-1}$ , than that of  $\text{OAc}^-$ ,  $\lambda^\circ(\text{OAc}^-) = 40.9$   $\text{cm}^2$   $\text{S mol}^{-1}$ ,<sup>72</sup> the greatest part is almost certainly due to the higher level of ion pair formation in  $\text{Mg}(\text{OAc})_2(\text{aq})$ . Greater association of  $\text{Mg}^{2+}$  with  $\text{OAc}^-$  cf.  $\text{NO}_3^-$  is also consistent with the reported activity coefficients of  $\text{Mg}(\text{OAc})_2(\text{aq})$ <sup>73</sup> and  $\text{Mg}(\text{NO}_3)_2(\text{aq})$ .<sup>74</sup>

The reasons why  $\text{OAc}^-$  associates with  $\text{Mg}^{2+}$  more strongly than does  $\text{NO}_3^-$  are undoubtedly complicated. In addition to long-range electrostatic interactions, short-range covalent and polarization effects are probably important. The effects of solvation must also be considered. Because of their very different structures and chemical characteristics, the interactions

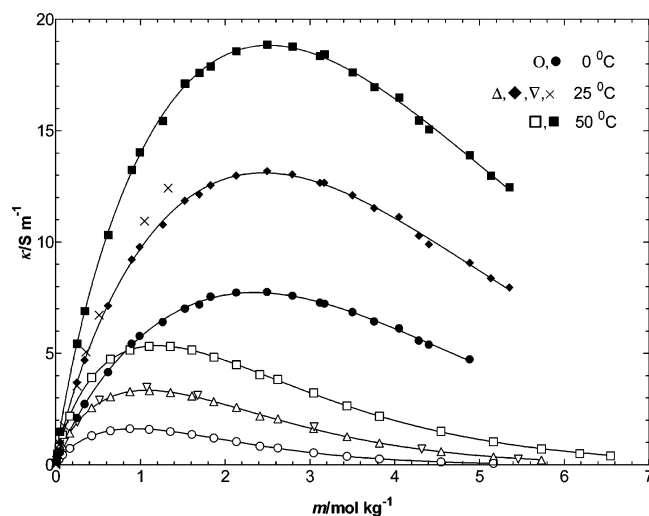


**Figure 7.** Variation of electrical conductivity with concentration for aqueous solutions of  $\text{Mg}(\text{OAc})_2$  (open symbols) and  $\text{Mg}(\text{NO}_3)_2$  (solid symbols) at three temperatures:  $\nabla$  ref 71a,  $\times$  ref 71b.

of  $\text{OAc}^-$  and  $\text{NO}_3^-$  with water molecules differ considerably. In the Hofmeister series,  $\text{OAc}^-$  lies toward the salting-out end whereas  $\text{NO}_3^-$  is toward the salting-in end, which indicates a very different interaction of the two ions with solvent water. Acetate is hydrated by six water molecules<sup>29</sup> and is thought to modify the structure of water in a manner similar to that caused by alcohols,<sup>75</sup> probably due to the presence of its hydrophobic part. On the other hand,  $\text{NO}_3^-$  forms a H-bonded complex with two water molecules having two dominant structures.<sup>76</sup> It may be that the hydrophobic end of the  $\text{CH}_3\text{COO}^-$  ion promotes its entry into the primary hydration shell of  $\text{Mg}^{2+}$ ; however, it should be noted that the “absolute” Gibbs energy of hydration for  $\text{OAc}^-$  is about 60  $\text{kJ mol}^{-1}$  more negative (i.e., more favorable) than that of  $\text{NO}_3^-$ .<sup>77</sup>

The differences between  $\text{Mg}(\text{OAc})_2(\text{aq})$  and  $\text{Mg}(\text{NO}_3)_2(\text{aq})$  for both  $\tau$  (Figure 6) and  $\kappa$  (Figure 7) become more pronounced at lower temperatures, which suggests that ion pairing in the former increases with decreasing temperature. This is consistent with the measured negative enthalpy of complexation.<sup>78</sup> It is interesting to note that the concentration corresponding to  $\kappa_{\text{max}}$  for  $\text{Mg}(\text{NO}_3)_2$  solutions coincides with the  $\kappa_s$  crossover. This is consistent with the presence of at least some types of ion pairs (probably noncontact) at higher concentrations.

**4.4. FT-Raman Spectra. 4.4.1. Magnesium Acetate Solutions.** The Raman spectra for  $\text{Mg}(\text{OAc})_2(\text{aq})$  are presented at various concentrations in Figure 8. The band positions associated with  $\text{OAc}^-$  are summarized in Table 4. Band assignments are based on those of previous investigations.<sup>8,32–35</sup> The antisymmetric stretching mode ( $\nu_8$ ) is only very weakly observed in Raman spectra and so will not be considered further.

The broad  $\text{COO}^-$  symmetric stretching mode ( $\nu_3$ ) of  $\text{OAc}^-$ , which appears in the 1400–1500  $\text{cm}^{-1}$  region (Figure 8), lies very close to, and contains contributions from, the  $\text{CH}_3$  deformation modes  $\nu_9$  and  $\nu_{13}$ .<sup>33,35,79</sup> This band shows a blue shift, with increasing intensity on the high-frequency side at higher salt concentrations, which is reflected in an increase in the full-width at half (maximum) height (fwhh) of the band (Table 4). At 5.410 mol  $\text{kg}^{-1}$ , two wings on the high-frequency side of this band are apparent at  $\sim 1445$  and  $\sim 1463$   $\text{cm}^{-1}$ . The  $\nu_3$ ,  $\nu_9$ , and  $\nu_{13}$  modes for solid  $\text{Mg}(\text{OAc})_2 \cdot 4\text{H}_2\text{O}$  also overlap. The resolved component bands were found to appear at 1436–1438, 1420–1421, and 1446–1455  $\text{cm}^{-1}$ , respectively.<sup>33,79</sup> In the solid phase, a bisacetato complex is the building unit for  $\text{Mg}(\text{OAc})_2$ .<sup>79,80</sup>

**TABLE 4: Peak Positions and Assignment of Modes Associated with the Acetate Ion in Aqueous Solutions of  $\text{Mg}(\text{OAc})_2$** 

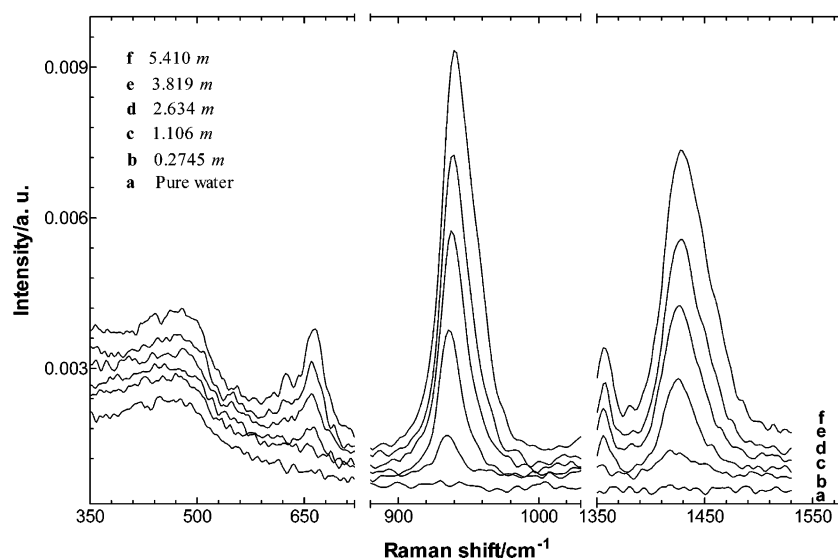
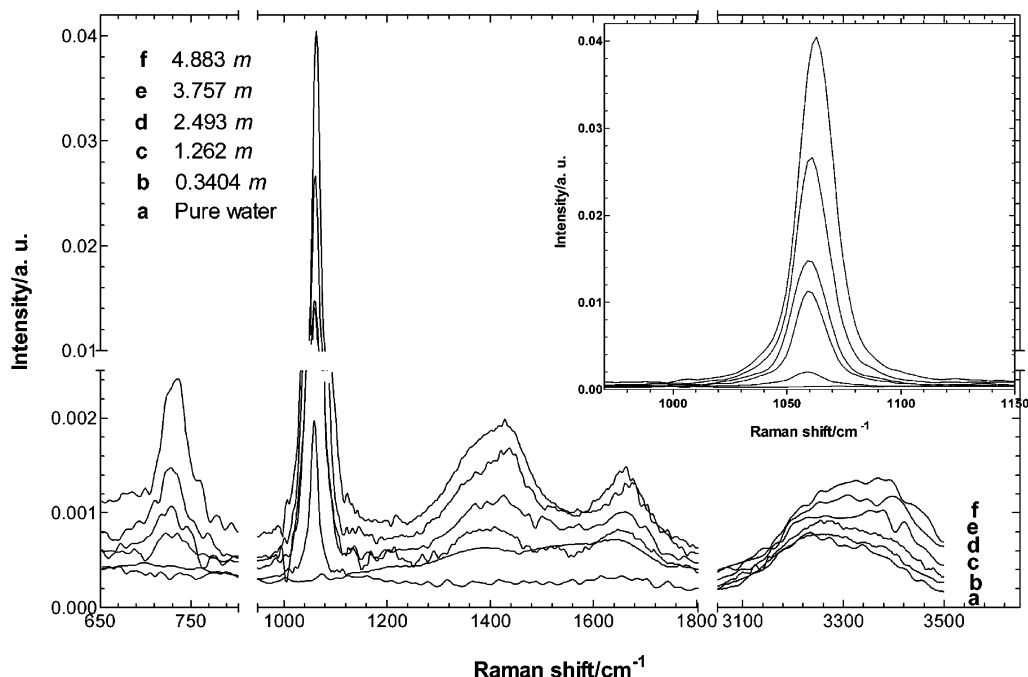
$m/\text{mol kg}^{-1}$	peak position/ $\text{cm}^{-1}$			
	$\text{COO}^-$ in-plane rock ( $\nu_{11}$ )	$\text{COO}^-$ deformation ( $\nu_5$ )	C—C stretch <sup>a</sup> ( $\nu_4$ )	$\text{COO}^-$ symmetric stretch <sup>a</sup> ( $\nu_3$ )
0.2745		654	935 (17)	1418 (32)
1.106		658	936 (19)	1425 (34)
2.634	480	660	938 (21)	1426 (39)
3.819	479	661	939 (24)	1428 (42)
5.410	479	666	940 (28)	1428 (45)

<sup>a</sup> The values in parentheses represent the full width at half-maximum height (fwhh) for the given band.

As the  $\text{CH}_3$  deformation modes ( $\nu_9$  and  $\nu_{13}$ ) are not sensitive to the metal–carboxyl group interactions, the observed frequency shift ( $\Delta\nu_3 \approx 10 \text{ cm}^{-1}$ ) and the increasing asymmetry of the band on the high-frequency side can be attributed to changes in the  $\text{COO}^-$  stretching vibration due to complexation with  $\text{Mg}^{2+}$ . Further, the appearance of the two high-frequency wings at  $5.410 \text{ mol kg}^{-1}$  suggests the occurrence of both mono- and bidentate complexes. Wang et al.<sup>35</sup> also observed two shoulders in the  $\nu_3$  Raman mode at  $\sim 1456$  and  $1443 \text{ cm}^{-1}$  at  $m$

$\geq 3.58 \text{ mol kg}^{-1}$  for  $\text{Mg}(\text{OAc})_2(\text{aq})$  and attributed them to bidentate and bridged bidentate complexes, respectively. Nickolov et al.<sup>33</sup> employed band fitting techniques to the Raman spectra of  $\text{Mg}(\text{OAc})_2(\text{aq})$  and reported that bisacetato complexes were the dominant species in saturated solutions.

The C—C stretching band ( $\nu_4$ ) of  $\text{OAc}^-$  is probably the most useful with respect to establishing the existence of metal–acetato complexes.<sup>33–35,79</sup> It has a high Raman scattering coefficient and does not overlap with other vibrations. In the present spectra

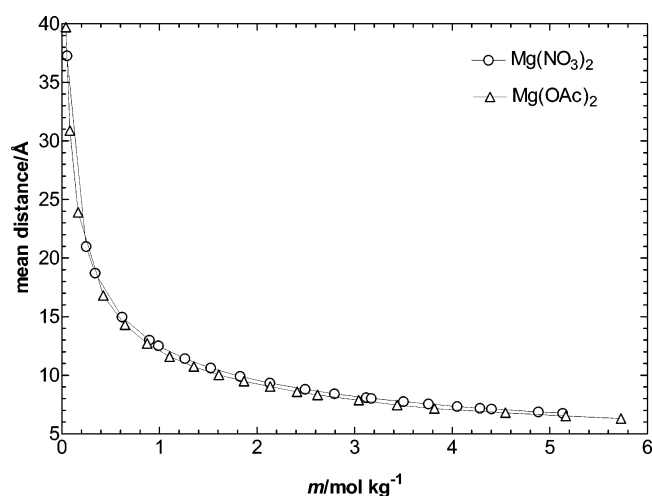
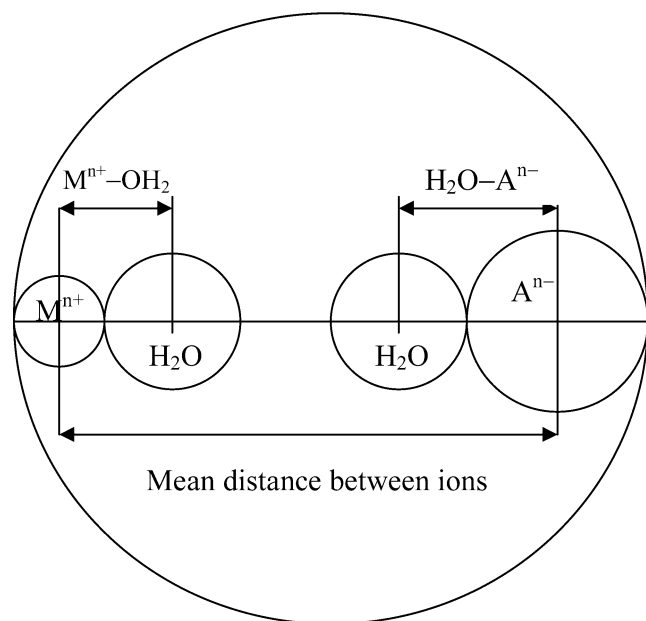
**Figure 8.** Raman spectra of aqueous solutions of  $\text{Mg}(\text{OAc})_2$  and pure water at room temperature.**Figure 9.** Raman spectra of aqueous solutions of  $\text{Mg}(\text{NO}_3)_2$  and pure water at room temperature.



**TABLE 5: Assignment of Modes and Peak Positions Associated with the Nitrate Ion in Aqueous Solutions of  $\text{Mg}(\text{NO}_3)_2$** 

$m/\text{mol kg}^{-1}$	peak position/ $\text{cm}^{-1}$				
	in-plane deformation ( $\nu_4$ )	symmetric stretch ( $\nu_1$ )	asymmetric stretch ( $\nu_3$ )	water O—H stretch	
0.3404	726	1059 (16)	1390	3234	3385
1.262	728	1059 (17)	1408	3259	3390
2.493	729	1059 (19)	1421	3254	3368
3.757	728	1061 (18)	1427	3260	3398
4.883	734	1063 (20)	1428	3264	3390

<sup>a</sup> The values in the parentheses represent the fwhh.

**Figure 10.** Variation of the mean cation–anion distance for  $\text{Mg}(\text{OAc})_2$ -(aq) and  $\text{Mg}(\text{NO}_3)_2$ -(aq) with concentration, assuming a random distribution of the ions.**Figure 11.** Geometrical representation of the separation between a cation,  $\text{M}^{n+}$  and an anion,  $\text{A}^{n-}$  in aqueous solutions.

(Figure 8), it occurs as a reasonably sharp band, centered at  $\sim 938 \text{ cm}^{-1}$ . As the solute concentration increases, this band shows a small blue shift (Table 4) and a simultaneous development of asymmetry on the high-frequency side with a weak shoulder at  $\sim 948 \text{ cm}^{-1}$ . The  $\nu_4$  band is observed at  $892 \text{ cm}^{-1}$  for  $\text{HOAc}$  and at  $928 \text{ cm}^{-1}$  for free  $\text{OAc}^-$ -(aq).<sup>34</sup> For  $\text{Mg}(\text{OAc})_2 \cdot 4\text{H}_2\text{O}(\text{s})$ , the band occurs at  $947 \text{ cm}^{-1}$ .<sup>33</sup> The variation in the position of the  $\nu_4$  mode with concentration suggests the

formation of mono- and bidentate contact ion pairs (inner-sphere complexes) at higher concentrations. Similar observations for  $\text{Mg}(\text{OAc})_2(\text{aq})$  have been made by Nickolov et al.<sup>33</sup> They resolved the  $\nu_4$  band into three components at 930, 939, and  $947 \text{ cm}^{-1}$  by curve fitting methods and ascribed them to free  $\text{OAc}^-$ , monoacetato complexes, and bisacetato complexes, respectively. A blue shift of the  $\nu_4$  band from 936 to  $947 \text{ cm}^{-1}$  with increasing concentration of  $\text{Mg}(\text{OAc})_2(\text{aq})$  was ascribed to the transformation of free  $\text{OAc}^-$  to contact ion pairs between  $\text{Mg}^{2+}$  and  $\text{OAc}^-$ .<sup>35</sup> Semmler et al.<sup>8</sup> suggested the formation of monoacetato complexes in  $\text{Mg}(\text{OAc})_2(\text{aq})$  and were able to resolve a band at  $939 \text{ cm}^{-1}$  above  $100^\circ \text{C}$ .

Additional evidence in support of complex formation in  $\text{Mg}(\text{OAc})_2$  solutions can be derived from the  $\text{COO}^-$  deformation or bending ( $\nu_5$ ) and in-plane rocking ( $\nu_{11}$ ) modes.<sup>79</sup> In the present spectra (Figure 8),  $\nu_5$  was observed at  $654 \text{ cm}^{-1}$  for a  $0.2745 \text{ mol kg}^{-1}$  solution, shifting to  $666 \text{ cm}^{-1}$  at  $5.410 \text{ mol kg}^{-1}$ . Such a large blue shift can be attributed to the complexation of  $\text{COO}^-$  with  $\text{Mg}^{2+}$ . However, at  $m \geq 2.634 \text{ mol kg}^{-1}$ , a shoulder appears at  $\sim 621 \text{ cm}^{-1}$ , ultimately producing a peak at  $624 \text{ cm}^{-1}$  at  $m = 5.410 \text{ mol kg}^{-1}$ . The appearance of two  $\nu_5$  bands is consistent with their observation (at 678 and  $612 \text{ cm}^{-1}$ ) for solid  $\text{Mg}(\text{OAc})_2$  at liquid nitrogen temperature.<sup>79</sup> This suggests that the  $624 \text{ cm}^{-1}$  band may originate from bidentate complexes.<sup>35</sup>

A broad envelope at  $400\text{--}500 \text{ cm}^{-1}$ , corresponding to the  $\nu_{11}$  mode, is observed (Figure 8) in the present spectra of  $\text{Mg}(\text{OAc})_2(\text{aq})$ . This band probably overlaps with the water libration band, which occurs at  $\sim 450 \text{ cm}^{-1}$ .<sup>81</sup> At higher concentrations ( $\geq 2.634 \text{ mol kg}^{-1}$ ), the  $\nu_{11}$  band becomes prominent at  $\sim 479 \text{ cm}^{-1}$ . Its broadness suggests the presence of various environments for the  $\text{COO}^-$  moiety. At  $5.410 \text{ mol kg}^{-1}$ , an additional shoulder at  $\sim 496 \text{ cm}^{-1}$  is apparent. This is identical to that reported for solid  $\text{Mg}(\text{OAc})_2 \cdot 4\text{H}_2\text{O}$ ,<sup>33</sup> which implies the presence of bisacetato complexes. A shift of the  $\nu_{11}$  mode from 480 to  $510 \text{ cm}^{-1}$  for aqueous  $\text{Ni}(\text{OAc})_2$  solutions has been ascribed to complex formation.<sup>82</sup>

**4.4.2. Magnesium Nitrate Solutions.** Raman spectra of  $\text{Mg}(\text{NO}_3)_2(\text{aq})$  are depicted in Figure 9. Unperturbed  $\text{NO}_3^-$  has  $D_{3h}$  symmetry and gives rise to symmetric stretching ( $\nu_1$ ), out-of-plane deformation ( $\nu_2$ ), asymmetric stretching ( $\nu_3$ ), and in-plane deformation or bending ( $\nu_4$ ) modes.<sup>21,22</sup> The  $\nu_3$  and  $\nu_4$  modes are both Raman and IR active, whereas the  $\nu_1$  is Raman active only and  $\nu_2$  is IR active only. The band positions for  $\text{NO}_3^-$  in the present  $\text{Mg}(\text{NO}_3)_2$  solutions are summarized in Table 5.

The inset in Figure 9 shows the variation of the  $\nu_1$  mode with increasing salt concentration. The intensity and the fwhh of this band increase as the concentration increases. The band position is constant at  $1059 \text{ cm}^{-1}$  up to  $2.493 \text{ mol kg}^{-1}$  but blue shifts by  $4 \text{ cm}^{-1}$  at higher concentrations. There is also a slight increase in the fwhh (Table 5), which has been attributed<sup>27</sup> to the influence of hydrated cations on  $\text{NO}_3^-$ . This implies the presence of noncontact ion pairs at high  $\text{Mg}(\text{NO}_3)_2$  concentrations. A previous study<sup>25</sup> of the Raman spectra of  $\text{Mg}(\text{NO}_3)_2$ -(aq) using principal component analysis indicated the presence of some associated species, probably a solvent-shared ion pair at  $\geq 2.5 \text{ mol dm}^{-3}$ .

Zhang et al.,<sup>23</sup> in their study of highly concentrated droplets of  $\text{Mg}(\text{NO}_3)_2(\text{aq})$  using Raman microscopy, observed that  $\nu_1$  shifted from  $1049$  to  $1055 \text{ cm}^{-1}$  when the concentration changed from  $7.60$  to  $10.09 \text{ mol kg}^{-1}$  and suggested it was due to the formation of contact ion pairs. Peleg<sup>21</sup> similarly reported  $\nu_1$  shifted from  $1049$  to  $1053 \text{ cm}^{-1}$  when the  $\text{Mg}(\text{NO}_3)_2$  concentration increased from  $9.25$  to  $13.22 \text{ mol kg}^{-1}$  and also invoked contact ion pairs as the explanation. Above  $9.25 \text{ mol kg}^{-1}$  (in



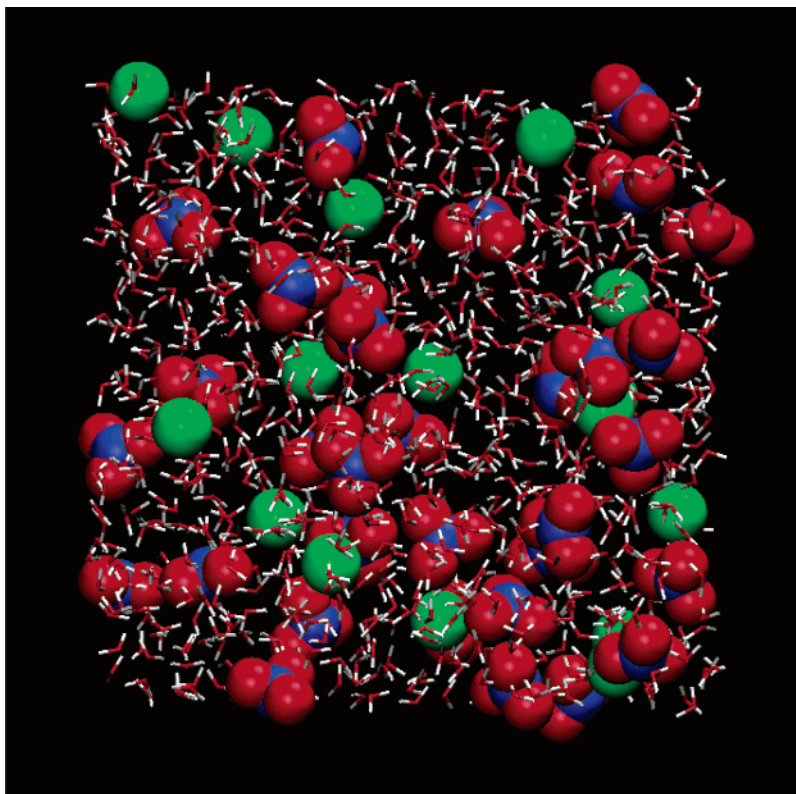


**Figure 12.** Snapshot from a simulation of 1 M  $\text{Mg}(\text{NO}_3)_2(\text{aq})$ . Color coding: Mg = green, N = blue, O = red, and H = white. For clarity, water molecules are displayed in stick representation.

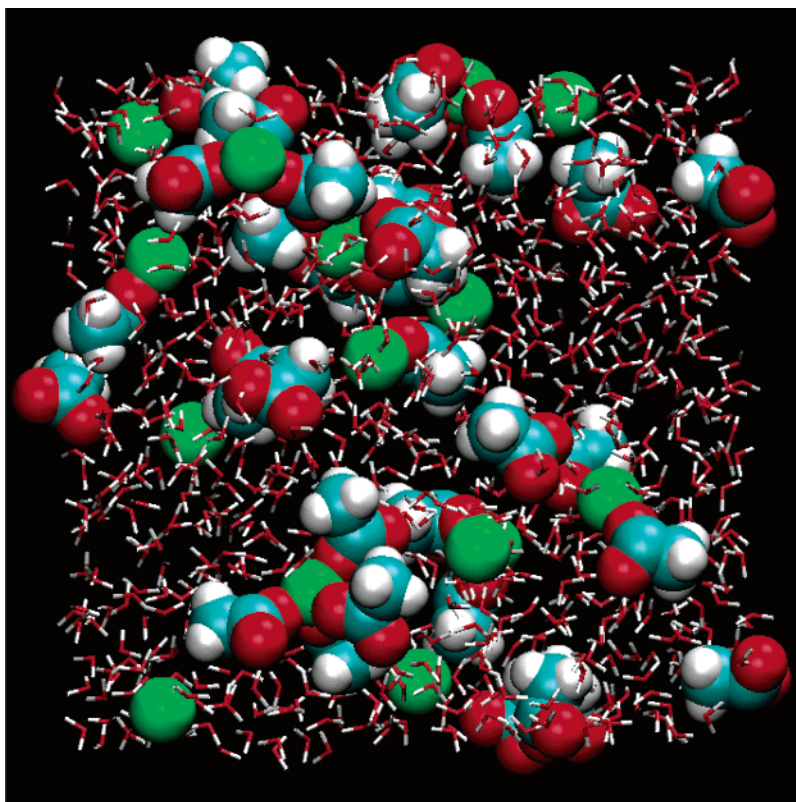


**Figure 13.** Snapshot from a simulation of 1 M  $\text{Mg}(\text{OAc})_2(\text{aq})$ . Color coding: Mg = green, C = cyan, O = red, and H = white. For clarity, water molecules are displayed in stick representation.

hydrated melts), splitting of the  $\nu_1$  band has been reported and was thought to be evidence for the formation of different types of contact ion pairs.<sup>21–23</sup>

Unperturbed  $\text{NO}_3^-$  gives a single  $\nu_3$  band at  $1370\text{ cm}^{-1}$ .<sup>76</sup> Previously,<sup>42,43,76,83</sup> it was concluded that water causes the

splitting of the  $\nu_3$  band due to hydration or solvent-shared ion pair formation. For example, bifurcated  $\nu_3$  bands appear at  $\sim 1341$  and  $\sim 1402\text{ cm}^{-1}$  in  $3.43\text{ mol kg}^{-1}\text{ Zn}(\text{NO}_3)_2(\text{aq})$ .<sup>42</sup> In the present study, no splitting of  $\nu_3$  was observed at lower concentrations and the band profiles matched well with those

of Chang and Irish<sup>22</sup> and Zhang et al.<sup>23</sup> At concentrations greater than  $2.493 \text{ mol kg}^{-1}$ , the band intensity increased asymmetrically on the high-frequency side and the band maximum occurred at  $\sim 1428 \text{ cm}^{-1}$  with a shoulder at  $\sim 1370 \text{ cm}^{-1}$ . Peleg<sup>21</sup> also reported a splitting of the  $\nu_3$  band in  $2.78 \text{ mol kg}^{-1}$   $\text{Mg}(\text{NO}_3)_2$  solutions. It seems reasonable to ascribe the  $\sim 1370 \text{ cm}^{-1}$  shoulder to unperturbed  $\text{NO}_3^-$ <sup>76</sup> and the mode at  $\sim 1428 \text{ cm}^{-1}$  to  $\text{NO}_3^-$  perturbed by (or associated with) hydrated cations.<sup>21</sup>

The intensity of the broad band in the  $1600\text{--}1700 \text{ cm}^{-1}$  region increases with concentration. However, as the  $2\nu_2$  overtone for  $\text{NO}_3^-$  at  $\sim 1658 \text{ cm}^{-1}$  and the water deformation mode (at  $1636 \text{ cm}^{-1}$ ) also occur in this region, no detailed analysis is possible.<sup>21,22</sup>

The appearance of double in-plane deformation bands ( $\nu_4$ ), at  $\sim 750$  and  $\sim 720 \text{ cm}^{-1}$ , is considered diagnostic for contact ion pair formation.<sup>20–22</sup> Our  $\text{Mg}(\text{NO}_3)_2$  solutions produced a single Raman band at  $\sim 726 \text{ cm}^{-1}$  for  $0.3404 \text{ mol kg}^{-1}$ , which blue shifted by only  $\sim 2 \text{ cm}^{-1}$  up to  $3.757 \text{ mol kg}^{-1}$ . The intensity of the band was proportional to the concentration.<sup>22</sup> At  $4.883 \text{ mol kg}^{-1}$ , the band shows a blue shift of  $\sim 8 \text{ cm}^{-1}$ , suggesting perturbation of  $\text{NO}_3^-$  by hydrated  $\text{Mg}^{2+}$ , as proposed by Angell.<sup>27</sup> The possible mode at  $\sim 760 \text{ cm}^{-1}$  (Figure 9) may be due to noise, because the  $750 \text{ cm}^{-1}$  band for  $\text{Mg}(\text{NO}_3)_2(\text{aq})$  appears only above  $9.25 \text{ mol kg}^{-1}$ .<sup>21,22</sup>

The  $\nu_{\text{O-H}}$  envelope of pure water is thought to consist of four components, an ice-like component ( $C_1$ ) at  $\sim 3230 \text{ cm}^{-1}$ , an ice-like liquid component ( $C_2$ ) at  $\sim 3420 \text{ cm}^{-1}$ , a liquidlike amorphous phase ( $C_3$ ) at  $\sim 3540 \text{ cm}^{-1}$ , and monomeric  $\text{H}_2\text{O}$  ( $C_4$ ) at  $\sim 3620 \text{ cm}^{-1}$ .<sup>84</sup> In the present systems, the  $\nu_{\text{O-H}}$  mode exhibits one broad peak at  $\sim 3234 \text{ cm}^{-1}$  with a shoulder at  $\sim 3385 \text{ cm}^{-1}$ . Upon addition of  $\text{Mg}(\text{NO}_3)_2$ , the shoulder grows relative to the  $\sim 3234 \text{ cm}^{-1}$  band. At  $4.883 \text{ mol kg}^{-1}$ , the shoulder becomes the main peak. The positive shift of the  $\nu_{\text{O-H}}$  band maximum has been ascribed to the disruption of the water structure and formation of bonds between water and ions.<sup>85</sup>

In summary, the Raman bands observed at  $\sim 726$ ,  $\sim 1059$ , and  $\sim 1390 \text{ cm}^{-1}$  along with  $\nu_{\text{O-H}}$  suggest that  $\text{NO}_3^-$  does not bond directly to  $\text{Mg}^{2+}$  within the experimental concentration range. Nevertheless, there are changes in the spectra that suggest that noncontact ion pairs may be formed, particularly at high concentrations. Clearly, as noted above, there are major differences between the extent and the nature (type) of the complex(es) formed in  $\text{Mg}(\text{OAc})_2(\text{aq})$  and  $\text{Mg}(\text{NO}_3)_2(\text{aq})$ . Although some interesting ideas have been proposed to account for such differences in general, see for example Collins<sup>86</sup> and Kiriukhin and Collins,<sup>87</sup> they are too speculative to warrant detailed discussion here.

**4.5. Mean Distance Between Cation and Anion.** To better ascertain the existence of different ionic species in different concentration regions, an attempt was made to determine the maximum possible mean cation–anion distance.<sup>88</sup> Assuming a random distribution of the ions in the solution without any attractive or repulsive interactions, the estimated mean cation–anion distance is depicted in Figure 10 as a function of concentration for both salt systems.

The mean cation–anion distance decreases sharply up to a solute concentration of  $\sim 1.0 \text{ mol kg}^{-1}$  according to this model but decreases gradually thereafter. A simple geometrical arrangement (Figure 11) illustrates the cation–anion separation, including water molecules: one nominally associated with the cation and another with the anion. For  $\text{Mg}(\text{OAc})_2(\text{aq})$ , the  $\text{Mg}^{2+}\text{--OH}_2$  and  $\text{OAc}^-\text{--}(\text{H}_2\text{O})$  equilibrium distances obtained from X-ray diffraction<sup>12,64</sup> should be taken into account along with the diameter of the water molecules. In Figure 11, the

separation is  $8.62 \text{ \AA}$ , which corresponds to the mean distance between the ions at a concentration of  $2.37 \text{ mol kg}^{-1}$ , if a random distribution without ion–ion interactions is assumed. Similarly for  $\text{Mg}(\text{NO}_3)_2(\text{aq})$ , the separation required by two water molecules between  $\text{Mg}^{2+}$  and  $\text{NO}_3^-$  is  $8.32 \text{ \AA}$ , which corresponds to the mean distance at  $2.86 \text{ mol kg}^{-1}$  (Figure 10). These concentrations,  $2.37$  and  $2.86 \text{ mol kg}^{-1}$  for  $\text{Mg}(\text{OAc})_2$  and  $\text{Mg}(\text{NO}_3)_2$ , respectively, are comparable with those at which  $\text{d}\kappa_s/\text{d}t = 0$  (Figure 5), which lends support to the idea that they correspond to the situation in which the available water molecules are just sufficient to complete the first hydration shells of the dissolved ions. Above these concentrations solvent-shared or contact ion pair formation is inevitable, as the mean separation between the ions can no longer accommodate more than one water molecule. It is again emphasized that this conclusion is derived from purely (and “primitive”) geometric considerations. No account has been taken of short-range attractive forces or even of geometric constraints, such as the presence of the  $\text{CH}_3$  group in the acetate ion, which might allow its closer approach to  $\text{Mg}^{2+}$ .<sup>35</sup>

**4.6. Computational Results.** Molecular dynamics simulations were used to study hydration and ion pairing in aqueous solutions of magnesium nitrate and acetate, yielding a statistically relevant picture with atomic resolution. Figures 12 and 13 present typical snapshots from simulations of  $1 \text{ M}$   $\text{Mg}(\text{NO}_3)_2$  and  $\text{Mg}(\text{OAc})_2(\text{aq})$ , which show the qualitative differences between these two salt systems. In  $\text{Mg}(\text{NO}_3)_2(\text{aq})$ , most of the ions are separated from other ions and are fully hydrated. The opposite is true for  $\text{Mg}(\text{OAc})_2(\text{aq})$ , where many of the  $\text{Mg}^{2+}$  ions are associated with  $\text{OAc}^-$  ions. Moreover, a significant

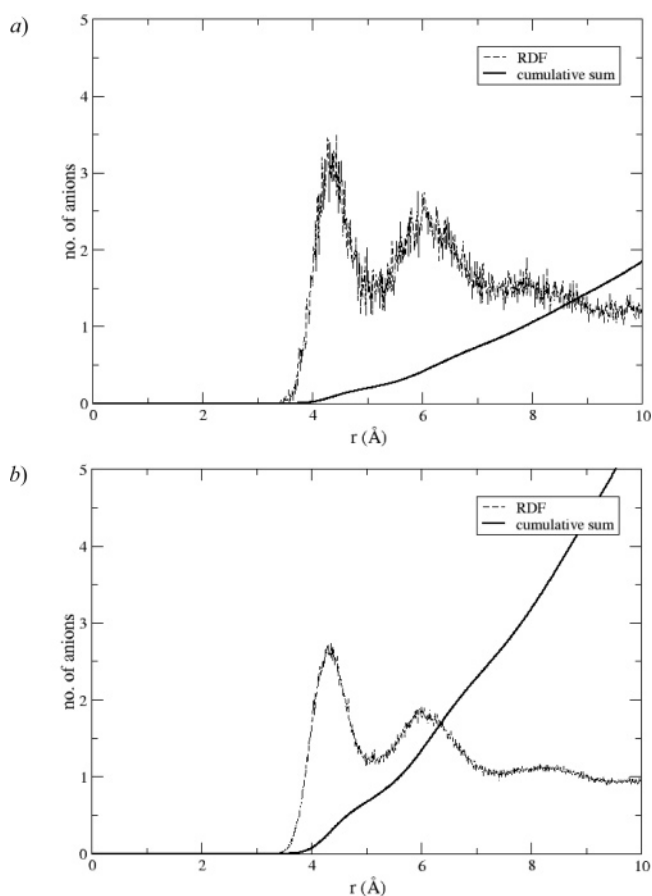


**Figure 14.** Magnesium–nitrate oxygen radial distribution function and cumulative sum for aqueous solutions at concentrations of (a)  $0.25 \text{ M}$  and (b)  $1 \text{ M}$ .

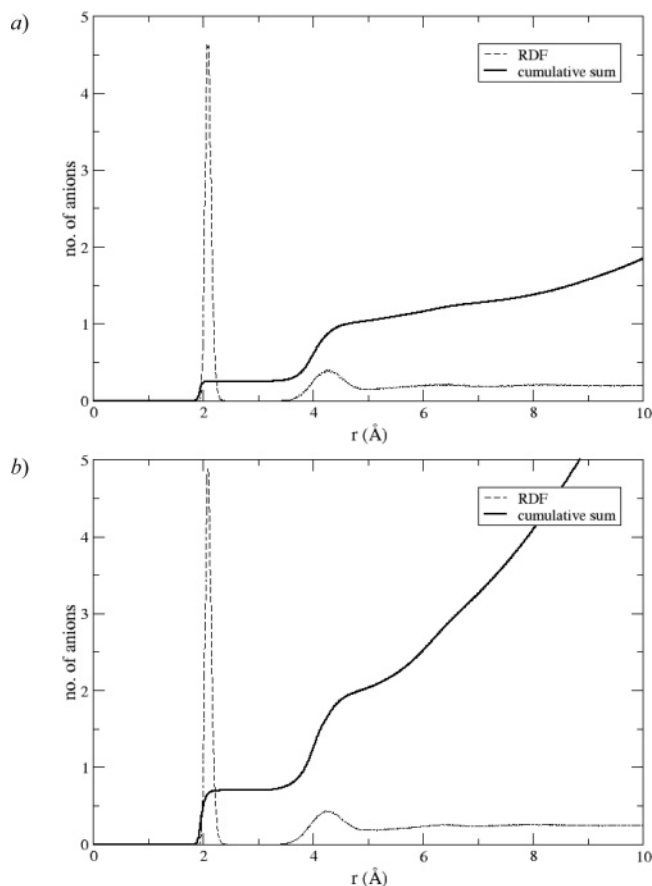


**Figure 15.** Magnesium–acetate oxygen radial distribution function and cumulative sum for aqueous solutions at a concentration of (a) 0.25 M and (b) 1 M.

degree of ion clustering is observed, particularly around  $\text{Mg}^{2+}$ , which is associated with more than one  $\text{OAc}^-$ .

The qualitative picture from the snapshots was quantified using statistically averaged (over nanosecond trajectories) data. In particular, the  $\text{Mg}^{2+}$ –anion and ion–water radial distribution functions (RDFs) were monitored, and cumulative sums were evaluated as integrals over these RDFs. The cumulative sums were normalized so as to provide the number of anions or water molecules within a particular distance from a given  $\text{Mg}^{2+}$ .

Figure 14 shows the magnesium–nitrate oxygen RDFs and cumulative sums for 0.25 and 1 M solutions. There are no contact ion pairs (which would correspond to a peak in the RDF at around 2.1 Å) present in either case. The RDF peak at 4.2 Å corresponds to ion pairs separated by one water molecule (i.e., a solvent-shared ion pair, SIP). There is also a broad feature at around 6 Å corresponding to ions separated by two water molecules (2 SIPs). It can be estimated from the cumulative sum that, on average, at 0.25 M, ~20% of  $\text{NO}_3^-$  is transiently associated with  $\text{Mg}^{2+}$  as SIPs. This rises to about 60% at 1 M.

Analogous information for the magnesium acetate solutions is presented in Figure 15. The situation is very different from the nitrate solutions: even at 0.25 M there is significant contact ion pairing, reflected in the RDF peak at around 2.1 Å. From the cumulative sum, it can be deduced that ~25% of  $\text{Mg}^{2+}$  forms contact ion pairs with  $\text{OAc}^-$ . Moreover, SIPs are also present (at around 4.2 Å). On average, there is one  $\text{OAc}^-$  per  $\text{Mg}^{2+}$  present either as contact ion pairs (CIPs) or as SIPs. At 1 M, this average rises to two, with ~0.7  $\text{OAc}^-$  per  $\text{Mg}^{2+}$  present as CIPs.

The ion–water distribution functions provide information about the concentration-dependent hydration patterns of the

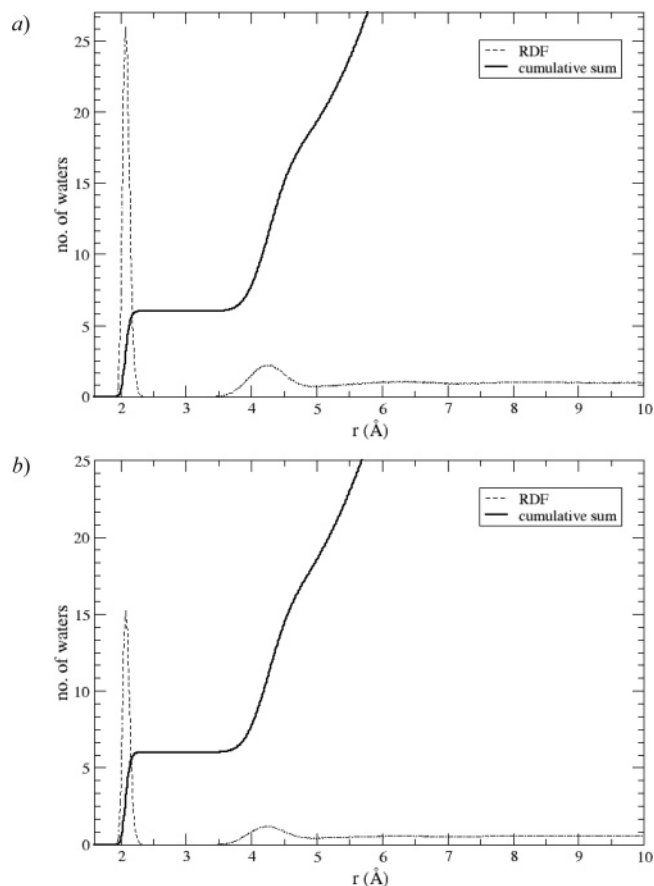


**Figure 16.** Magnesium–water oxygen radial distribution function and cumulative sum for aqueous solutions of magnesium nitrate at a concentration of (a) 0.25 M and (b) 1 M.

individual ions. Figure 16 shows the magnesium–water oxygen RDFs and the cumulative sum for 0.25 and 1 M solutions of  $\text{Mg}(\text{NO}_3)_2$ . For both concentrations, there is a rigid first hydration shell around  $\text{Mg}^{2+}$  containing six strongly bound water molecules, which is typical for alkaline-earth cations. The position of the first hydration shell peak at around 2.1 Å agrees very well with X-ray diffraction experiments.<sup>89</sup> A broader peak at around 4.2 Å marks a much “softer” second solvation shell containing roughly 12 water molecules. The existence of a second hydration sheath around  $\text{Mg}^{2+}$  containing 12 water molecules is consistent with both dielectric relaxation measurements<sup>90</sup> and vibrational spectra.<sup>91</sup>

The magnesium–water oxygen RDFs and the cumulative sums for  $\text{Mg}(\text{OAc})_2(\text{aq})$ , depicted in Figure 17, are affected by strong ion pairing. Thus, the number of water molecules in the first hydration shell drops from 6 to approximately 5.6 at 0.25 M and to 4.8 at 1 M, consistent with them being partially replaced by acetate anions. On average, about one water molecule is displaced from the first hydration shell of  $\text{Mg}^{2+}$  in 1 M  $\text{Mg}(\text{OAc})_2$ .

Test calculations employing polarizable potentials gave very similar results to the nonpolarizable simulations concerning the structure of the solutions and ion pairing. If anything, the tendency for ion pairing increased upon the inclusion of polarization. This is demonstrated, for example, in Figure 18, which shows the magnesium–acetate oxygen RDF and cumulative sum for the 0.25 M solution containing polarizable ions and water molecules. It can be seen that the results compare semiquantitatively to the results employing a nonpolarizable force field (see Figure 15a), except that the direct ion pairing is slightly enhanced.



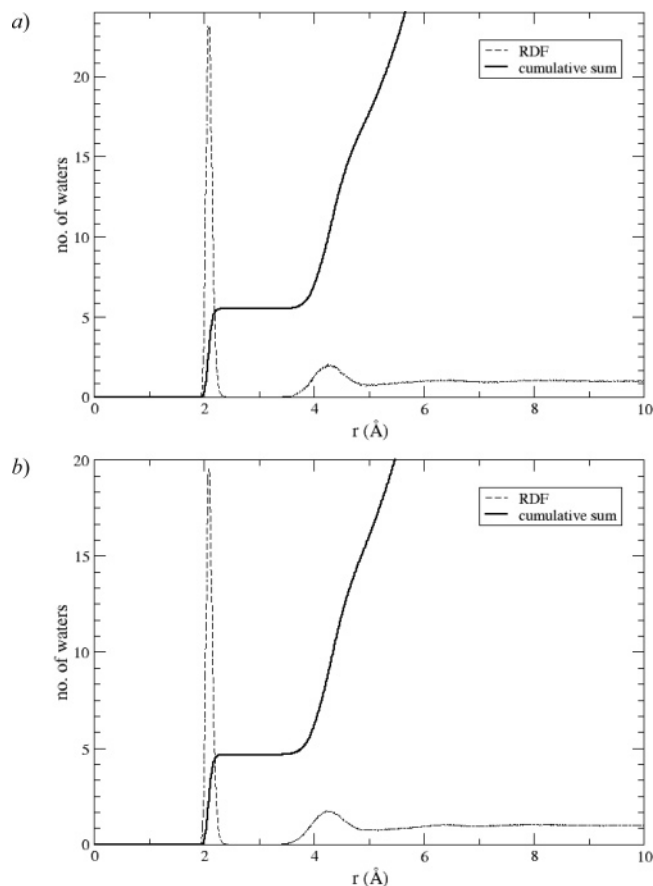


**Figure 17.** Magnesium–water oxygen radial distribution function and cumulative sum for aqueous solutions of magnesium acetate at a concentration of (a) 0.25 M and (b) 1 M.

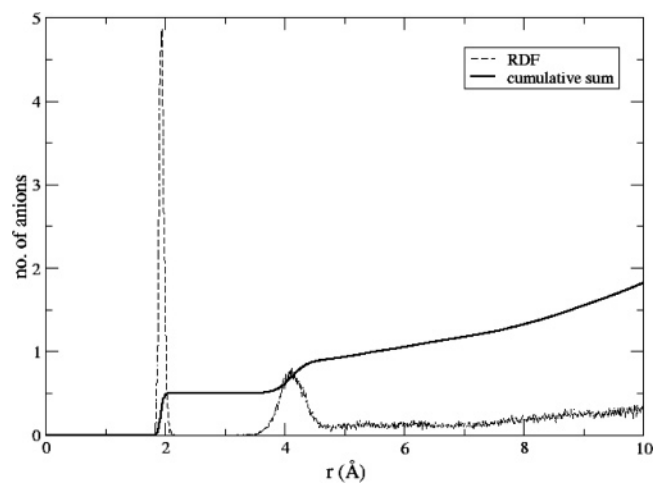


**Figure 18.** Magnesium–acetate oxygen radial distribution function and cumulative sum for an aqueous solution at a concentration of 0.25 M employing polarizable potentials.

## 5. Conclusions

Ionic charge density, especially of cations, appears to be a major factor influencing the isentropic compressibilities of aqueous electrolyte solutions. However, the present data for  $\text{Mg}(\text{OAc})_2$  and  $\text{Mg}(\text{NO}_3)_2$  solutions along with literature values for other salts indicate that anion effects follow the Hofmeister series. The significant differences, which exist between  $\text{Mg}(\text{OAc})_2$  and  $\text{Mg}(\text{NO}_3)_2$  solutions, with respect to their structural relaxation times, viscosities, and electrical conductivities, are consistent with a much greater degree of ion association in the former. This is confirmed by the Raman spectra of  $\text{Mg}(\text{OAc})_2$ -

(aq), which show substantial changes with concentration, consistent with the formation of mono- and bidentate complexes (contact ion pairs), whereas for  $\text{Mg}(\text{NO}_3)_2(\text{aq})$  only noncontact ion pairs are implied. The mean cation–anion separation estimated from a simple geometrical approach suggests that the electrolyte concentration at which  $\text{d}\kappa_s/\text{d}r = 0$  (Figure 5) corresponds to the disappearance of bulk water from the solution. The experimental results are supported by MD simulations of 0.25 and 1 M solutions of magnesium nitrate and acetate. These simulations indicate, in accord with experiment, that contact ion pairs are absent in  $\text{Mg}(\text{NO}_3)_2$  solutions, where only solvent-separated ion pairs (SIPs and 2 SIPs, the total number of which rises steeply with concentration) can be observed. In contrast, CIPs are prevalent in  $\text{Mg}(\text{OAc})_2$  solutions at both concentrations. The number of CIPs and SIPs increases strongly with concentration, and at 1 M, a significant ion clustering occurs. This is also reflected in the structure of the first hydration shell around  $\text{Mg}^{2+}$ , from which on average about one water molecule is replaced by acetate.

**Acknowledgment.** A.W. and S.M. are grateful to the Director, Regional Research Laboratory, Jorhat, India for interest in this work, and A.W. is thankful to the Council of Scientific and Industrial Research, New Delhi, India for the award of senior research fellowship. Support (to P.J.) from the Czech Ministry of Education (Grant LC512) and from the U.S. NSF (Grants CHE 0431512 and 0209719) is gratefully acknowledged. The authors are also grateful to the Sophisticated Analytical Instrumentation Facility, Indian Institute of Technology-Madras, India for recording the Raman spectra.

## References and Notes

- (1) Grossfield, A.; Ren, P.; Ponder, J. W. *J. Am. Chem. Soc.* **2003**, *125*, 15671.
- (2) Tieleman, D. P.; Biggin, P. C.; Smith, G. R.; Sansom, M. S. P. *Q. Rev. Biophys.* **2001**, *34*, 473.
- (3) Hille, B. *Ionic Channels of Excitable Membranes*, 3rd ed.; Sinauer Associates Inc.: Sunderland, MA, 2001.
- (4) Shvartsburg, A. A.; Siu, K. W. M. *J. Am. Chem. Soc.* **2001**, *123*, 10071.
- (5) Lippard, S. J. *Science* **1993**, *261*, 699.
- (6) Lide, D. R., Ed. *Handbook of Chemistry and Physics*, 76th ed.; CRC Press: Boca Raton, FL, 1995; p XIV – 11.
- (7) Berthelin, J. *Pedologie* **1982**, *32*, 313.
- (8) Semmler, J.; Irish, D. E.; Oseki, T. *Geochim. Cosmochim. Acta* **1990**, *54*, 947.
- (9) Oum, K. W.; Lakin, M. J.; Dehaan, D. O.; Brauers, T.; Finlayson-Pitts, B. J. *Science* **1998**, *279*, 74.
- (10) Bol, W.; Gerrits, G. J. A.; van Panthaleon van Eck, C. L. *Appl. Crystallogr.* **1970**, *3*, 486.
- (11) Bulmer, J. T.; Irish, D. E.; Ödberg, L. *Can. J. Chem.* **1975**, *53*, 3806.
- (12) Caminiti, R.; Licheri, G.; Piccaluga, G.; Pinna, G. *Chem. Phys. Lett.* **1979**, *61*, 45.
- (13) Ohtaki, H.; Radnai, T. *Chem. Rev.* **1993**, *93*, 1157.
- (14) Markham, G. D.; Glusker, J. P.; Bock, C. L.; Trachtman, M.; Bock, C. W. *J. Phys. Chem.* **1996**, *100*, 3488.
- (15) Pavlov, M. P.; Siegbahn, E. M.; Sandström, M. *J. Phys. Chem. A* **1998**, *102*, 219.
- (16) Pye, C. C.; Rudolph, W. W. *J. Phys. Chem. A* **1998**, *102*, 9933.
- (17) Righellato, E. C.; Davies, C. W. *Trans. Faraday Soc.* **1930**, *26*, 592.
- (18) Robinson, R. A.; Wilson, J. M.; Ayling, H. S. *J. Am. Chem. Soc.* **1942**, *64*, 1469.
- (19) Vollmar, P. M. *J. Chem. Phys.* **1963**, *39*, 2236.
- (20) Irish, D. E.; Chang, T. G.; Nelson, D. L. *Inorg. Chem.* **1970**, *9*, 425.
- (21) Peleg, M. *J. Phys. Chem.* **1972**, *76*, 1019.
- (22) Chang, T. G.; Irish, D. E. *J. Phys. Chem.* **1973**, *77*, 52.
- (23) Zhang, Y.-H.; Choi, M. Y.; Chan, C. K. *J. Phys. Chem. A* **2004**, *108*, 1712.
- (24) James, D. W.; Carrick, M. T.; Frost, R. L. *J. Raman Spectrosc.* **1982**, *13*, 115.
- (25) Tomišić, V.; Simeon, V. *Phys. Chem. Chem. Phys.* **2000**, *2*, 1943.



- (26) James, D. W.; Frost, R. L. *Aust. J. Chem.* **1982**, *35*, 1793.
- (27) Angell, C. A. *J. Electrochem. Soc.* **1965**, *112*, 1224.
- (28) Irish, D. E.; Nelson, D. L.; Brooker, M. H. *J. Chem. Phys.* **1971**, *54*, 654.
- (29) Caminiti, R.; Cucca, P.; Monduzzi, M.; Saba, G.; Crisponi, G. *J. Chem. Phys.* **1984**, *81*, 543.
- (30) Shehata, H. A. *J. Chem. Soc., Faraday Trans.* **1994**, *90*, 3401.
- (31) Purdie, P.; Barlow, A. J. *J. Chem. Soc., Faraday Trans. 2* **1972**, *68*, 33.
- (32) Tackett, J. E. *Appl. Spectrosc.* **1989**, *43*, 483.
- (33) Nickolov, Zh.; Ivanov, I.; Georgiev, G.; Stoilova, D. *J. Mol. Struct.* **1996**, *377*, 13.
- (34) Quilès, F.; Burneau, A. *Vib. Spectrosc.* **1998**, *16*, 105.
- (35) Wang, L.-Y.; Zhang, Y.-H.; Zhao, L.-J. *J. Phys. Chem. A* **2005**, *109*, 609.
- (36) Hofmeister, F. *Naum-Schmiedeberg's Archiv. Exp. Pathol. Pharmacol.* **1888**, *23*, 247. English translation: Kunz, W.; Henle, J.; Ninham, B. W. *Curr. Opin. Colloid Interface Sci.* **2004**, *9*, 19.
- (37) (a) Cacace, M. G.; Landau, E. M.; Ramsden, J. J. *Q. Rev. Biophys.* **1997**, *30*, 241. (b) Kunz, W.; Lo Nostro, P.; Ninham, B. W. *Curr. Opin. Colloid Interface Sci.* **2004**, *9*, vii.
- (38) Kunz, W.; Lo Nostro, P.; Ninham, B. W. *Curr. Opin. Colloid Interface Sci.* **2004**, *9*, 1.
- (39) Marcus, Y. *Ion Solvation*; John Wiley & Sons: Chichester, U.K., 1985.
- (40) (a) Omta, A. W.; Kropman, M. F.; Woutersen, S. *J. Chem. Phys.* **2003**, *119*, 12457. (b) Omta, A. W.; Kropman, M. F.; Woutersen, S.; Bakker, H. J. *Science* **2003**, *301*, 347. (c) Näslund, L.-Å.; Edwards, D. C.; Wernet, P.; Bergmann, U.; Ogasawara, H.; Pettersson, L. G. M.; Myneni, S.; Nilsson, A. *J. Phys. Chem. A* **2005**, *109*, 5995.
- (41) Vogel, A. I. *Textbook of Quantitative Inorganic Analysis*; 4th ed.; ELBS: Longman, U.K., 1985; p 316.
- (42) Wahab, A.; Mahiuddin, S. *J. Chem. Eng. Data* **2004**, *49*, 126.
- (43) Rohman, N.; Wahab, A.; Mahiuddin, S. *J. Solution Chem.* **2005**, *34*, 77.
- (44) Rohman, N.; Dass, N. N.; Mahiuddin, S. *J. Chem. Eng. Data* **1999**, *44*, 465.
- (45) Allen, M. P.; Tildesley, D. J. *Computer Simulations of Liquids*; Clarendon: Oxford, U.K., 1987.
- (46) Essmann, U.; Perera, L.; Berkowitz, M. L.; Darden, T.; Lee, H.; Pedersen, L. G. *J. Chem. Phys.* **1995**, *103*, 8577.
- (47) Ryckaert, J.-P.; Cicciotti, G.; Berendsen, H. J. C. *J. Comput. Phys.* **1977**, *23*, 327.
- (48) Thole, B. T. *Chem. Phys.* **1981**, *59*, 341.
- (49) Vrbka, L.; Mucha, M.; Minofar, B.; Jungwirth, P.; Brown, E. C.; Tobias, D. J. *Curr. Opin. Colloid Interface Sci.* **2004**, *9*, 67.
- (50) Berendsen, H. J. C.; Grigera, J. R.; Straatsma, T. P. *J. Phys. Chem.* **1987**, *91*, 6269.
- (51) Wang, J. M.; Wolf, R. M.; Caldwell, J. M.; Kollman, P. A. *J. Comput. Chem.* **2004**, *25*, 1157.
- (52) Jorgensen, W. L. *OPLS and OPLS-AA Parameters for Organic Molecules, Ions, and Nucleic Acids*, Yale University, New Haven, CT, 1997.
- (53) Frisch, M. J.; Trucks, G. W.; Schlegel, H. B.; Scuseria, G. E.; Robb, M. A.; Cheeseman, J. R.; Montgomery, J. A., Jr.; Vreven, T.; Kudin, K. N.; Burant, J. C.; Millam, J. M.; Iyengar, S. S.; Tomasi, J.; Barone, V.; Mennucci, B.; Cossi, M.; Scalmani, G.; Rega, N.; Petersson, G. A.; Nakatsuji, H.; Hada, M.; Ehara, M.; Toyota, K.; Fukuda, R.; Hasegawa, J.; Ishida, M.; Nakajima, T.; Honda, Y.; Kitao, O.; Nakai, H.; Klene, M.; Li, X.; Knox, J. E.; Hratchian, H. P.; Cross, J. B.; Bakken, V.; Adamo, C.; Jaramillo, J.; Gomperts, R.; Stratmann, R. E.; Yazyev, O.; Austin, A. J.; Cammi, R.; Pomelli, C.; Ochterski, J. W.; Ayala, P. Y.; Morokuma, K.; Voth, G. A.; Salvador, P.; Dannenberg, J. J.; Zakrzewski, V. G.; Dapprich, S.; Daniels, A. D.; Strain, M. C.; Farkas, O.; Malick, D. K.; Rabuck, A. D.; Raghavachari, K.; Foresman, J. B.; Ortiz, J. V.; Cui, Q.; Baboul, A. G.; Clifford, S.; Cioslowski, J.; Stefanov, B. B.; Liu, G.; Liashenko, A.; Piskorz, P.; Komaromi, I.; Martin, R. L.; Fox, D. J.; Keith, T.; Al-Laham, M. A.; Peng, C. Y.; Nanayakkara, A.; Challacombe, M.; Gill, P. M. W.; Johnson, B.; Chen, W.; Wong, M. W.; Gonzalez, C.; Pople, J. A. *Gaussian 03*; Gaussian, Inc.: Wallingford CT, 2004.
- (54) Case, D. A.; Darden, T. A.; Cheatham, T. E., III; Simmerling, C. L.; Wang, J.; Duke, R. E.; Luo, R.; Merz, K. M.; Wang, B.; Pearlman, D. A.; Crowley, M.; Brozell, S.; Tsui, V.; Gohlke, H.; Mongan, J.; Hornak, V.; Cui, G.; Beroza, P.; Schafmeister, C.; Caldwell, J. W.; Ross, W. S.; Kollman, P. A. *AMBER 8*; University of California: San Francisco, CA, 2004.
- (55) Caldwell, J.; Kollman, P. A. *J. Phys. Chem.* **1995**, *99*, 6208.
- (56) Wang, J. M.; Cieplak, P.; Kollman, P. A. *J. Comput. Chem.* **2000**, *21*, 1049.
- (57) Petersen, P. B.; Mucha, M.; Jungwirth, P.; Saykally, R. J., *J. Phys. Chem. B* **2005**, *109*, 10915.
- (58) Emara, M. M.; Farid, N. A. *J. Indian Chem. Soc.* **1981**, *58*, 474.
- (59) Doan, T. H.; Sangster, J. *J. Chem. Eng. Data* **1981**, *26*, 141.
- (60) Mahiuddin, S.; Ismail, K. *Can. J. Chem.* **1982**, *60*, 2883.
- (61) Behrends, R.; Miecznik, P.; Kaatz, U. *J. Phys. Chem. A* **2002**, *106*, 6039.
- (62) Phillips, C. G.; Williams, R. J. P. *Inorganic Chemistry*; Clarendon Press: New York, 1965; Vol. 1, p 161.
- (63) Marcus, Y.; Hefter, G. *Chem. Rev.* **2004**, *104*, 3405.
- (64) Ohtaki, H. *Monatsh. Chem.* **2001**, *132*, 1237.
- (65) Millero, F. J.; Ricco, J.; Schreiber, D. R. *J. Solution Chem.* **1982**, *11*, 671.
- (66) Desnoyers, J. E.; Perron, G. *J. Solution Chem.* **1972**, *1*, 199.
- (67) Jenkins, H. D. B.; Marcus, Y. *Chem. Rev.* **1995**, *95*, 2695.
- (68) Rohman, N.; Mahiuddin, S. *J. Chem. Soc., Faraday Trans.* **1997**, *93*, 2053.
- (69) Rohman, N.; Dass, N. N.; Mahiuddin, S. *J. Mol. Liq.* **2002**, *100* (3), 265.
- (70) Gurney, R. W. *Ionic Processes in Solutions*; Dover Publications: New York, 1953.
- (71) *International Critical Tables of Numerical Data, Physics, Chemistry and Technology*; Washburn, E. W., Ed.; McGraw-Hill: New York, 1928; (a) Vol. VI, p 254. (b) Vol. VI, p 238.
- (72) Harned, H. S.; Owen, B. B. *The Physical Chemistry of Electrolytic Solutions*; 2nd ed.; Reinhold Publishing Corporation: New York, 1950; p 172.
- (73) Strokes, R. H. *J. Am. Chem. Soc.* **1953**, *75*, 3856.
- (74) Todorov, M.; Ninkov, R. *J. Chem. Thermodyn.* **1995**, *27*, 369.
- (75) Koga, Y.; Westh, P.; Davies, J. V.; Miki, K.; Nishikawa, K.; Katayanagi, H. *J. Phys. Chem. A* **2004**, *108*, 8533.
- (76) Waterland, M. R.; Stockwell, D.; Kelley, A. M. *J. Chem. Phys.* **2001**, *114*, 6249.
- (77) Marcus, Y. *Ion Properties*; Marcel Dekker: New York, 1997.
- (78) Nancollas, G. H. *J. Chem. Soc.* **1956**, 744.
- (79) Frost, R. L.; Klopogge, J. T. *J. Mol. Struct.* **2000**, *526*, 131.
- (80) Padmanabhan, A. C.; Srinivasan, R. *Indian J. Pure Appl. Phys.* **1973**, *11*, 404.
- (81) Hester, R. E.; Plane, R. A. *Spectrochim. Acta* **1967**, *23A*, 2289.
- (82) Bickley, R. I.; Edwards, H. G. M.; Rose, S. J.; Guster, R. *J. Mol. Struct.* **1990**, *238*, 15.
- (83) Irish, D. E.; Davis, A. R. *Can. J. Chem.* **1968**, *46*, 943.
- (84) Zhang, Y.-H.; Chan, C. K. *J. Phys. Chem. A* **2003**, *107*, 5956.
- (85) Walrafen, G. E. *J. Chem. Phys.* **1962**, *36*, 1035.
- (86) Collins, K. D. *Biophys. J.* **1997**, *72*, 65.
- (87) Kiriukhin, M. Y.; Collins, K. D. *Biophys. Chem.* **2002**, *99*, 155.
- (88) For example, a 1 M Mg(OAc)<sub>2</sub> solution is considered where the water molecules are taken as hard spheres of radius 1.4 Å. The ionic radii of Mg<sup>2+</sup> and OAc<sup>-</sup> are taken as 0.65 and 2.32 Å, and the corresponding volumes would be 1.15 and 52.31 Å<sup>3</sup>, respectively. At this concentration, ions would constitute a volume fraction of 6.37%. Now, a spherical box is taken to fill it randomly with the particles (ions) so that 6.37% is occupied. The maximum possible mean distance between a cation and an anion along the diameter of the sphere is calculated to be 11.72 Å.
- (89) Marcus, Y. *Chem. Rev.* **1988**, *88*, 1475.
- (90) Buchner, R.; Chen, T.; Hefter, G. T. *J. Phys. Chem. B* **2004**, *108*, 2365.
- (91) Rudolph, W. W.; Irmer, G.; Hefter, G. T. *Phys. Chem. Chem. Phys.* **2003**, *5*, 5253.